# SECONDARY CELLS WITH LITHIUM ANODES AND IMMOBILIZED FUSED-SALT ELECTROLYTES

H. Shimotake, G. L. Rogers, and E. J. Cairns

Argonne National Laboratory
9700 South Cass Avenue
Argonne, Illinois
60439

## Introduction

Today's rapidly-advancing technology requires a wide spectrum of power sources and energy-storage devices. In many applications, the power sources are required to have a minimum size or weight per unit of power or energy. These requirements have motivated a great deal of the recent work on high-specific-energy (watt-hr/lb) and high-specific-power (watt/lb) secondary cells. The maximization of the specific energy requires that reactants of low equivalent weight and high free energy of reaction be used. For high specific energy (> 50 watt-hr/lb) cells with aqueous electrolytes, zinc and cadmium have served as anode materials while nickel oxide, silver oxide, and oxygen (or air) have served as cathode materials.[1,2,3] The elimination of water from the electrolyte permits more reactive metals such as calcium and the alkali metals to be considered as anode materials. Lithium has a very low equivalent weight and low electronegativity, making it particularly attractive as an anode material for high specific energy cells. A number of cathode materials have been used in combination with nonaqueous electrolytes and lithium anodes, depending on the operating temperature and the electrolyte.

Lithium-anode cells designed for operation at room temperature use nonaqueous electrolytes comprised of solutions of inorganic salts such as $Li_3PF_4$ or $LiClO_4$ dissolved in organic solvents such as propylene carbonate or dimethyl sulfoxide; the cathodes are usually metal halides such as $NiF_4$, $CuF_2$ or CuCl.[1,3] Although these cells have the potentiality of supplying over 100 watt-hr/lb at low discharge rates, their specific power is low (2-20 watt/lb),[1,3] limiting their range of applicability. The specific power for cells with organic-solvent electrolytes is low because of the low conductivity of the electrolyte ($\sim 10^{-2}$ ohm$^{-1}$ cm$^{-1}$).

The use of fused-salts as electrolytes provides very high conductivities (1-4 ohm$^{-1}$ cm$^{-1}$) thus allowing specific powers in excess of 100 watt/lb to be achieved.[4-8] Because of their relatively high melting points, fused-salt electrolytes require elevated operating temperatures (260-650°C). A number of secondary cells with fused-salt electrolytes have been investigated, including sodium/bismuth,[9] lithium/chlorine,[7,8] lithium/tellurium,[4-6] and lithium/selenium,[10] all using free liquid electrolytes.

A general indication of the theoretical maximum specific energies of some couples suitable for use with fused-salt electrolytes is given in Figure 1, where the specific energy (as calculated from the equivalent weight of the cell products indicated and the average emf of the couple) is plotted against the equivalent weight of the active material. Usually, the higher specific energy materials are more difficult to handle from a corrosion viewpoint.

A great deal of design flexibility and compactness can be gained by immobilizing the fused-salt electrolyte either in an absorbent matrix or in the form of a rigid paste.[11-13] This work deals with secondary cells having liquid lithium anodes, liquid bismuth or tellurium cathodes and fused-lithium-halide electrolytes immobilized as a rigid paste, operating at temperatures in the range 380 to 485°C.

## Experimental

Typical lithium/bismuth and lithium/tellurium cells are shown in Figures 2 and 3. The cell housing in Figure 2 was made from Type 316 stainless steel; the electrode compartments were 3.2 mm deep, and had 4 concentric fins which

served as current collectors. The exposed electrolyte area was 1.98 $cm^2$, and the paste electrolyte thickness was 0.34 cm. Prior to assembly, the anode compartment was loaded with 0.064 gm of lithium (Foote Mineral Co., 0.003 % Na, 0.003% K, 0.003% $N_2$, 0.003% $Cl_2$, surface oxide removed), heated to 530°C to ensure good wetting of the current collector. The cathode compartment contained 2.764 gm of bismuth (United Mineral and Chemical Corp., 99.999% minimum purity). These amounts of reactants correspond to a cathode-alloy composition of 41 a/o Li in Bi at complete discharge, and a cell capacity of 0.25 amp-hr. The cell was prepared and assembled under a high-purity helium atmosphere.[14] No gaskets were used; the smooth-surfaced electrolyte disc provided a leak-tight seal against the cell housing.

The lithium/tellurium cell, made of pure iron, had current collectors consisting of sheets of sintered porous stainless steel in the anode compartment, and a network of pure-iron wires in the cathode compartment in place of the meshes shown in Figure 3. The exposed electrolyte area was 3.25 $cm^2$; the electrolyte thickness was 0.32 cm. The cell compartments were loaded with 0.75 gm of lithium and 5.45 gm of tellurium, (American Smelting and Refining Co., 99.999% minimum purity) corresponding to 71.6 a/o Li in Te at complete discharge.

The electrolyte was the ternary eutectic composed of 11.7 m/o LiF - 29.1 m/o LiCl - 59.2 m/o LiI, which melts at 340.9°C and has a specific conductance of 2.3 $ohm^{-1}$ $cm^{-1}$ at 375°C and 3.0 $ohm^{-1}$ $cm^{-1}$ at 475°C.[15] The eutectic was prepared from weighed amounts of the pure salts: LiF, LiCl, and LiI all supplied by Anderson Physics Laboratories, Inc. After the components were melted together to form the eutectic, the electrolyte was solidified, pulverized to -300 mesh, and mixed (50 w/o) with an inert filler material. The electrolyte-filler powder mixture was then molded into discs. For the Li/Bi cell, discs 1.85 cm in dia. were prepared by pressing the electrolyte-filler powder first at room temperature to form "cold-pressed" discs, and then at 400°C for final densification. All operations except for the hot-pressing were carried out in a pure helium atmosphere. For the Li/Te cell, discs 2.5 cm in dia. were pressed at room temperature and sintered at 400°C without pressing, eliminating all exposure to air.

The paste electrolyte has a continuous phase of fused-lithium-halide eutectic at the cell operating temperature. The relative amounts of finely-divided inert filler and lithium halide are chosen such that the electrolyte fills the interstitial spaces among the very small filler particles, and holds the paste firmly by means of its high surface tension, low contact angle with the filler, and the small pore size of the compact. Similar paste electrolytes have been used with success in molten-carbonate fuel cells.[11-13]

The measurements of cell performance were carried out with the aid of a constant-current DC power supply, precision voltmeters and ammeters (1/4 percent), and a strip-chart recorder. The voltage-current density curves for the discharge mode of operation were measured starting with the cell in the fully-charged condition; the curves for the charge mode of operation were usually measured from the fully-discharged condition. All results are reported on a resistance-included basis. The cells were held at operating temperature in an electrically-heated tube furnace.

## Results and Discussion

The voltage-current density curves for the Li/Bi cell operating at 380°, 453°, and 485°C are shown in Figure 4. As might be expected, the highest performance in both charge and discharge modes was obtained at the highest temperature. Current densities up to 2.2 amp/$cm^2$ were obtained, based on the effective electrode area of 1 $cm^2$ (the electrode compartments were only about half-filled with active materials during these experiments). Since the cathode composition during the discharge experiments averaged about 5 a/o Li,[16] these performances are typical of those obtainable near the beginning of the plateau of the corresponding voltage-

time curves at constant current discharge. The maximum power density at 485°C was 0.57 watt/cm$^2$ at 0.6 volt.

The slopes of the charge and discharge curves in Figure 4 are different because of the difference in state of charge for the two modes of operation. The internal resistance of the cell is expected to be lower for the discharge curves because most of the original amount of lithium was still in the anode compartment when the discharge data were taken. During the charging experiments, however, almost no lithium was present in the lithium compartment, resulting in a relatively high internal resistance. When charge and discharge curves are taken under identical conditions, the curves have the same slope. The internal resistance of the cell at high current densities was 0.45 ohm at 485°C, compared to a value of 0.23 ohm calculated from the specific conductance of the electrolyte and a paste-to-pure electrolyte resistivity ratio of 2.[11,13] This discrepancy could be caused by the presence of some $Li_2O$ resulting from hydrolysis of the lithium halides during hot-pressing or incomplete wetting of the paste by Li.

From the reasonably high current density capabilities of the Li/Bi cell of Figure 4, it is clear that the cell can be fully charged from complete discharge in about 15 minutes.

The performance characteristics of the (larger) Li/Te cell operating at 475°C are shown in Figure 5. As expected on the basis of the emf measurements of Foster and Liu[17] and earlier experience with Li/Te cells,[4-6] the open circuit voltage was 1.7 to 1.8 volts, and the voltage-current density curves were straight lines, indicating the absence of any significant concentration or activation overvoltages. The short-circuit current density was 2.2 amp/cm$^2$, and the maximum power density was 1 watt/cm$^2$ at 0.9 volt, a considerable improvement in power density over the Li/Bi cell.

The internal resistance of the Li/Te cell during discharge was 0.24 ohm, compared to 0.065 ohm calculated from the electrolyte conductivity and a paste-to-pure electrolyte resistivity ratio of 2. The ratio of observed-to-calculated cell resistances is higher for the Li/Te cell than for the Li/Bi cell, possibly because of the fact that the paste electrolyte disc for the Li/Te cell was not hot-pressed, and therefore probably contained voids which increased the resistivity of the paste.

The Li/Te cell, with a capacity of 2.91 amp-hr could be fully charged from complete discharge in less than half an hour. This is a much higher charge rate than can be used with secondary cells having aqueous electrolytes or cells with nonaqueous organic solvent electrolytes.

Extensive investigations of constant-current charge and discharge characteristics, charge retention, and cycle life still remain to be done. The data presented above were interesting enough, however, that some preliminary design calculations have been performed, based upon the voltage-current density curves of Figures 4 and 5.

The principles, equations, and sample calculations involved in the design of secondary batteries have already been discussed elsewhere[4], therefore, no detailed explanations will be given here. The most important parameter in many applications is battery weight; therefore, the energy and power values are expressed per unit weight as specific energy (watt-hr/lb) and specific power (watt/lb). The calculation of battery weight involves the selection of the ratio of reactant weights, and the calculation of the weights of reactants, electrolyte, cell housing, terminals, etc. required, per unit of active cell area. The specific power available is calculated from the current density-voltage curve and the battery weight per unit active area. The specific energy is calculated from the average cell operating voltage, the amount of lithium per unit of active cell area and the battery weight per unit of active area.[4] The values used in these calculations are summarized in Table I.

The results of the design calculations for Li/Bi and Li/Te secondary batteries are shown in Figure 6. Because of the lower equivalent weight and higher electronegativity, the Li/Te cell has higher specific energy and specific power capabilities than the Li/Bi cell. As an example, Figure 6 shows that for the 30-minute-discharge rate, a Li/Bi cell having 3 cells per inch and an electrolyte thickness of 0.32 cm has a specific power of 43 watt/lb and a specific energy of 21 watt-hr/lb, whereas the Li/Te cell of similar dimensions can attain 110 watt/lb and 55 watt-hr/lb. The design analysis results presented in Figure 6 also indicate that if the electrolyte thickness is decreased to 0.1 cm, it is possible to achieve 90 watt/lb and 45 watt-hr/lb for the Li/Bi cell and 200 watt/lb and 110 watt-hr/lb for the Li/Te cell. The performances of some other types of secondary batteries including lead-acid, nickel/cadmium, sodium/sulfur, and lithium/chlorine are presented in Figure 6 for comparison.

Possible applications for secondary cells with the characteristics of the Li/Te cell include space power sources, military communications power sources, military vehicle propulsion, and perhaps special commercial vehicle propulsion.[5]

The areas which deserve further attention in the development of Li/Bi and Li/Te cells include the optimization of paste electrolyte properties (particularly the resistivity), current collection, corrosion, cycle life, and thermal cycling.

## Conclusions

1. It is possible to form acceptable paste electrolytes from fused-lithium halides and inert filler materials. The paste electrolytes presently show two to three times the expected electrolytic resistivities.

2. Lithium/bismuth and lithium/tellurium cells operating with lithium halide paste electrolytes can operate at power densities of 0.57 and 1.0 watt/cm$^2$, respectively at about 480°C.

3. These cells can be charged at very high rates (less than 30 minutes), making them possible candidates for many applications where fast recharge is important.

4. Design calculations indicate that the Li/Te cell with paste electrolyte can be expected to show a specific power in excess of 360 watt/lb and a specific energy of 80 watt-hr/lb, suggesting many possible applications, including special vehicle propulsion and energy storage.

## Acknowledgment

It is a pleasure to thank Mr. J. Gerard for help with some of the experiments, and Drs. A. D. Tevebaugh, C. E. Johnson, and M. S. Foster for helpful discussions during the course of this work. Mr. B. S. Baker of the Institute of Gas Technology generously provided advice and materials on the preparation of paste electrolytes.

## References


1. R. Jasinski, "High-Energy Batteries", Plenum Press, New York (1967).

2. A. M. Moos and N. I. Palmer, in *Proc. 21st Ann. Power Sources Conf.*, PSC Publications Committee, Red Bank, New Jersey (1967).

3. H. N. Seiger, S. Charlip, A. E. Lyall and R. C. Shair, in *Proc. 21st Ann. Power Sources Conf.*, PSC Publications Committee, Red Bank, New Jersey (1967).

4. H. Shimotake and E. J. Cairns, Presented at the Intersociety Energy Conversion Engineering Conf., Miami Beach, August, 1967, in *Advances in Energy Conversion Engineering*, Amer. Soc. Mech. Eng., New York (1967), p. 951.

5. E. J. Cairns and H. Shimotake, Presented at Amer. Chem. Soc. Meeting, Chicago, September 1967, Abstr. No. L-70; See also *Preprints of Papers Presented to the Division of Fuel Chemistry 11*, No. 3, 321 (1967).

6. H. Shimotake, G. L. Rogers, and E. J. Cairns, Presented at Electrochem. Soc. Meeting, Chicago, October, 1967, Abstr. No. 18; See also *Extended Abstracts J-1 of the Battery Div., 12*, 42 (1967).

7. R. A. Rightmire and A. L. Jones, in *Proc. 21st Ann. Power Sources Conf.*, PSC Publications Committee, Red Bank, New Jersey (1967).

8. H. A. Wilcox, in *Proc. 21st Ann. Power Sources Conf.*, PSC Publications Committee, Red Bank, New Jersey (1967).

9. H. Shimotake and E. J. Cairns, Presented at Electrochem. Soc. Meeting, Dallas, May, 1967, Abstr. No. 143; See also *Extended Abstrs. of the Industrial Electrolytic Div., 3*, 4 (1967).

10. H. Shimotake and E. J. Cairns, Submitted for Presentation at the International Power Sources Symposium, Brighton, September, 1968.

11. G. H. J. Broers and M. Schenke, in "Fuel Cells", Vol. 2, G. J. Young, Ed., Reinhold, New York (1963).

12. B. S. Baker, L. G. Marianowski, J. Zimmer and G. Price, in "Hydrocarbon Fuel Cell Technology", B. S. Baker, Ed., Academic Press, New York (1965).

13. A. D. S. Tantram, A. C. C. Tseung, and B. S. Harris, in "Hydrocarbon Fuel Cell Technology", B. S. Baker, Ed., Academic Press, New York (1965).

14. C. E. Johnson, M. S. Foster, and M. L. Kyle, *Nuclear Appl., 3*, 563 (1967).

15. C. E. Johnson, Submitted for Presentation at the San Francisco Meeting of The Amer. Chem. Soc., Apr., 1968.

16. M. S. Foster, S. E. Wood, and C. E. Crouthamel, *Inorg. Chem., 3*, 1428 (1964).

17. M. S. Foster and C. C. Liu, *J. Phys. Chem., 70*, 950 (1966).

Table I

Data for Battery Design Calculations

| | Li/Bi | Li/Te |
|---|---|---|
| Open-circuit voltage, volts | 0.8 | 1.7 |
| Short-circuit current density, amp/cm$^2$ | | |
| for electrolyte thickness 0.3 cm | 1.8 | 2.2 |
| for electrolyte thickness 0.1 cm | 6.1 | 7.0 |
| Cathode alloy, fully discharged | | |
| composition, a/o Li | 70 | 60 |
| density, g/cm$^3$ | 4.4 | 3.3 |
| Anode metal density, g/cm$^3$ | 0.53 | 0.53 |
| Current efficiency, % | 100 | 100 |
| Cell partition thickness, cm/cell | 0.1 | 0.1 |
| Density of housing material, g/cm$^3$ | 7.8 | 7.8 |
| Density of paste electrolyte, g/cm$^3$ | 3.0 | 3.0 |
| Weight allowance for framing, terminals, etc. % (electrolyte + partition weight) | 50 | 50 |

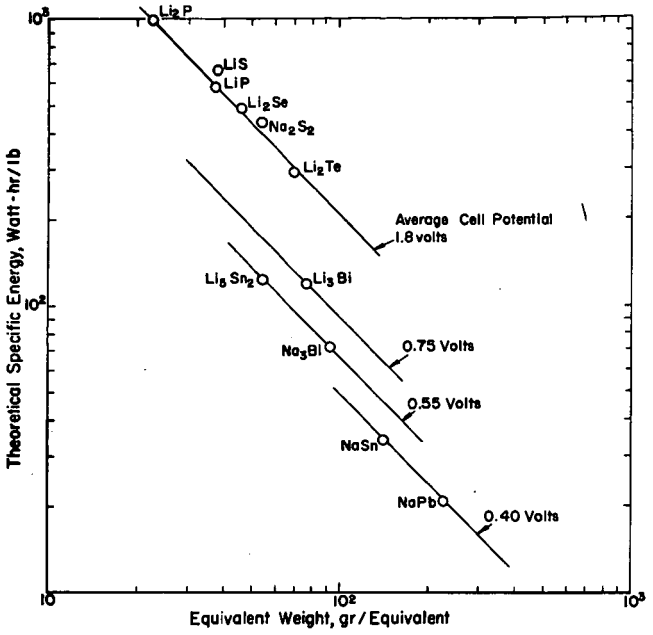


Fig. 1. Relationship between theoretical specific energy and equivalent weight

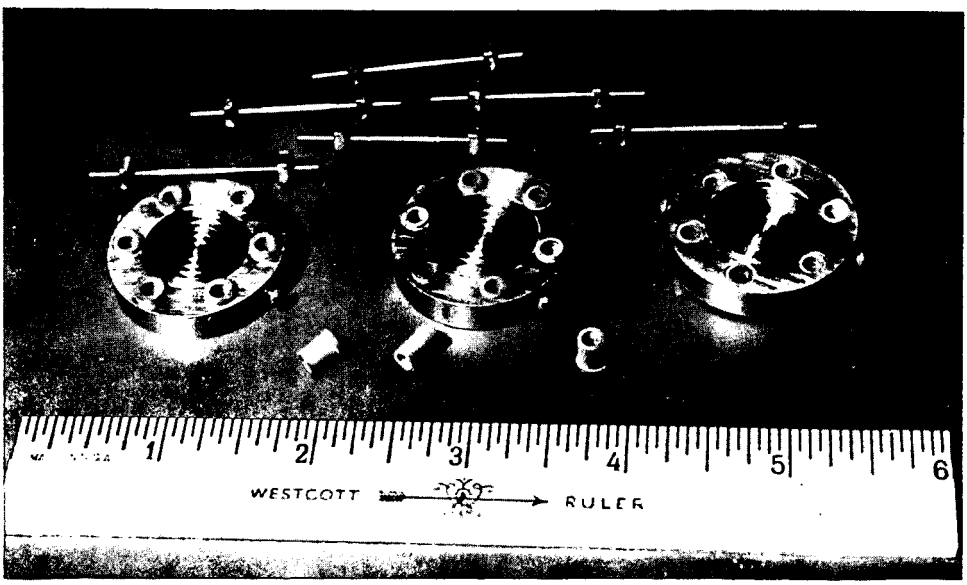


Fig. 2. View of lithium-bismuth-cell parts. Enough cell parts to make a two-cell battery are shown.

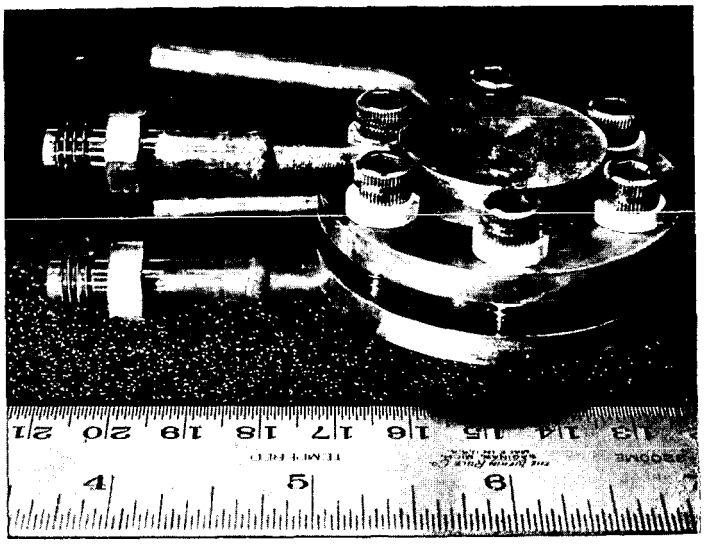

Fig. 3a. View of assembled lithium-tellurium cell

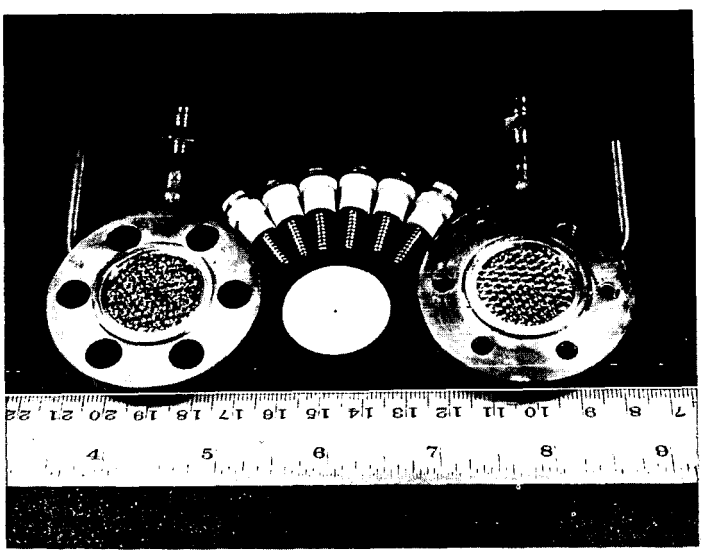

Fig. 3b. View of lithium-tellurium-cell parts

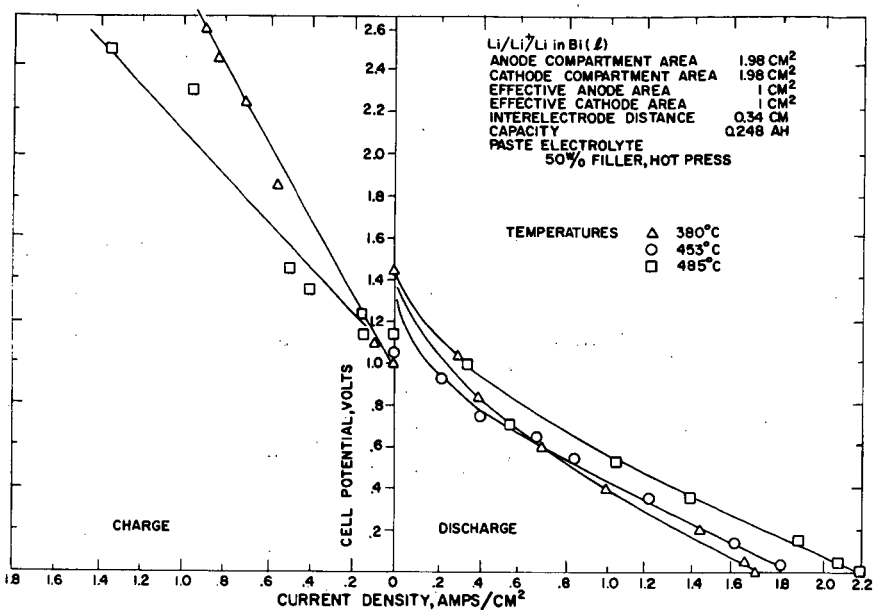


Fig. 4. Voltage-current density curves for a lithium-bismuth cell

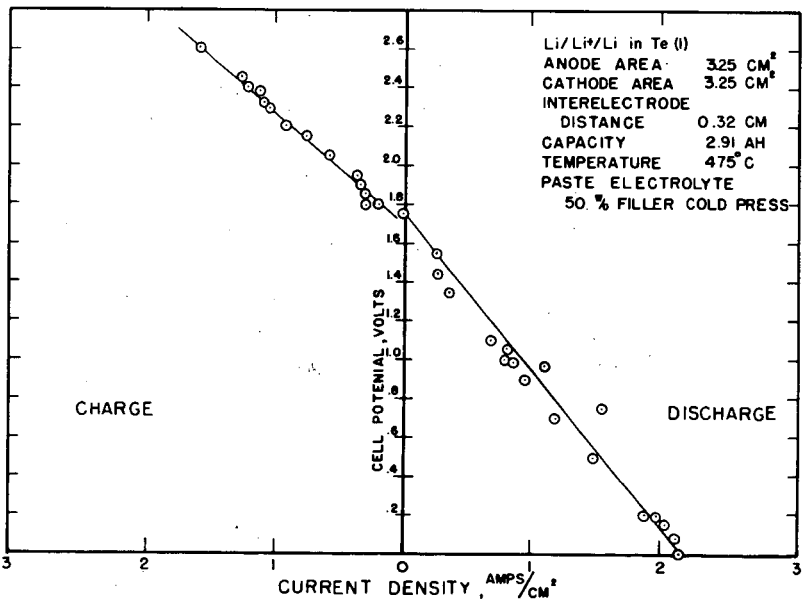


Fig. 5. Voltage-current density curves for a lithium-tellurium cell

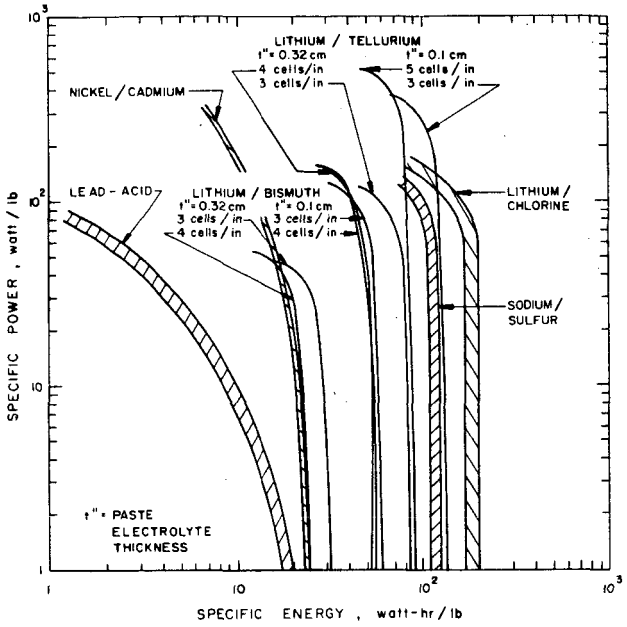


Fig. 6. Specific power-specific energy curves for some secondary batteries

# COAL PYROLYSIS USING LASER IRRADIATION

F. S. Karn, R. A. Friedel, and A. G. Sharkey, Jr.

U.S. Department of the Interior, Bureau of Mines
Pittsburgh Coal Research Center, Pittsburgh, Pa. 15213

## INTRODUCTION

The purpose of this investigation is to observe the effect of laser irradiation on the pyrolysis of coal. Coal irradiated with laser light can decompose into gases rich in acetylene. Coal pyrolysis at the usual coking temperatures yields gases high in methane but very low in acetylene. The acetylene/methane ratio and the probable commercial value of the product gas should be related directly to the temperature of the decomposing coal.

Conventional coal pyrolysis varies in temperature from 450° to 1,400°C and includes hundreds of different processes and coals. A typical high-temperature pyrolysis gas was obtained from a Pittsburgh seam (hvab) coal carbonized at 900° C.[5] Fifteen percent of the coal (40.7 percent volatile matter) was collected as gas (table 1). Laser irradiation can bring about significant changes in the $C_2H_2/CH_4$ ratio by increasing pyrolysis temperature. The equilibrium constant for the reaction

$$2CH_4 \rightleftharpoons C_2H_2 + 3H_2$$

increases from $10^{-7}$ at 1,000° K to $10^{+9}$ at 4,000° K. Temperatures resulting from laser irradiation could be very high. The energy concentration due to a 6-joule focused beam from a ruby laser is sufficient to raise the temperature of a perfect absorber by 14,000° C. This estimate is based on the laser energy and on the heat capacity of the target. However, much of the laser energy is dissipated by reflection, conduction, and vaporization. In these experiments with coal the maximum target temperature was estimated to be less than 1,300° K--largely due to coal volatility. Interesting observations of target temperatures of laser-irradiated solids have been reported. Berkowitz and Chupka[1] analyzed the vapor ejected from graphite and found it compatible with an assumption of thermodynamic equilibrium and a temperature of 4,000° K. Verber and Adelman,[7] using tantalum as a target, measured thermionic emission due to a surface temperature increase which was calculated from classical heat transfer theory. In the following experiments temperatures have not been measured directly due to the small size of the coal crater and to the rapid heating and cooling of the sample.

## EXPERIMENTAL

A variety of coals and coal macerals have been exposed to laser irradiation. Using a focused beam, energy concentrations as high as 100 megawatts per square centimeter can be reached. The general procedure has been to seal the coal sample in a glass vessel through which the laser beam can be fired. The vessel was evacuated or evacuated and partially refilled with a specific gas before irradiation. Samples, usually about 8 mm cubes, were sealed in glass tubes 10 mm i.d. and 90 mm long.[6] Samples were dried under vacuum at 100° C for 20 hours, then sealed and irradiated. The usual irradiation was 1 pulse of a 6-joule ruby laser beam which was focused by a convex lens. Gaseous products were analyzed by the mass spectrometer in two or more fractions distilling from liquid nitrogen, dry ice, ice water, room temperature, and 60° C baths. Both total volume and gas distribution were determined for each fraction. Solid products were obtained from the glass walls for ultimate analysis or for inspection by infrared spectrometry.

Table 1.- Product gas

| | 900°C carbonization | Laser irradiation |
|---|---|---|
| | Mole percent | |
| $H_2$ | 55.6 | 52.2 |
| CO | 7.4 | 22.5 |
| $CO_2$ | 0.4 | 8.7 |
| $CH_4$ | 31.5 | 5.1 |
| $C_2H_2$ | 0.05 | 10.6 |
| $C_2H_4$ | 3.4 | 0.0 |
| $C_2H_6$ | 1.2 | 0.0 |
| $> C_2$ | 0.5 | 0.0 |
| HCN | 0.0 | 0.9 |
| | Weight percent of coal | |
| | 15 | 52 |
| | $C_2H_2/CH_4$ | |
| | < 0.002 | 2.1 |

In studying any new process for coal pyrolysis, there are several useful variables to be considered. Among these are coal rank, maceral, particle size, and atmosphere. There are also several variables which are characteristic of the processing unit. For the laser they are quantity of energy discharged, rate of discharge, area of target, and wavelength of radiant energy.

Coals have been treated with the same total light energy from 3 different lasers. Lasers used in these experiments were as follows: The ruby laser delivers 6 joules of 6,943 A light in about 1 millisecond. Source of the light is a cylindrical ruby 76 mm long by 6.3 mm in diameter. It is activated by a xenon flash lamp and a capacitor capable of delivering a 2,000-volt pulse. The neodymium laser is a glass rod 152 mm long and capable of a 28-joule pulsed discharge. The third laser type is a continuous $CO_2$ laser. Its total power output is only 10 watts (10 joules/sec) but since it operates continuously the total energy and the quantity of product gas can be made to equal that of the pulsed lasers. Irradiation from the $CO_2$ laser has a wavelength of 106,000 A.

## RESULTS

A comparison of product gases from a 900° C carbonization and from irradiation by a ruby laser verified the prediction of higher $C_2H_2$ to $CH_4$ ratio for the laser (table 1).

Rank. Coal composition and coal utilization vary widely with rank. Irradiation products as a function of rank were studied earlier and the results are summarized in table 2.[3/] As rank decreases the yield of gaseous product increases. Yields of acetylene, hydrogen, and HCN reach a maximum for a high-volatile bituminous coal.

Macerals. Macerals from a single coal seam can be separated visually or by specific gravity. They provide information about the origin of a coal and about its coking properties. Maceral separation is a tedious job and well separated samples are usually small.[2/] Macerals of Hernshaw (hvab) coal in sufficient quantity for laser pyrolysis were irradiated (table 3). As hydrogen and volatile matter in the maceral increased the product gas increased, and the quality of the product gas (based on $C_2H_2/CH_4$ ratio) decreased.

Table 2.- Product gases from laser irradiation of coals

| | Anthracite | Pocahontas lvb | Pittsburgh hvab | Lignite |
|---|---|---|---|---|
| | Moles x $10^7$ | | | |
| $H_2$ | 13 | 23 | 30 | 21 |
| CO | 8 | 5 | 12 | 24 |
| $CO_2$ | 4 | 1 | 3 | 10 |
| $CH_4$ | 1 | 1 | 3 | 1 |
| $C_2H_2$ | 3 | 4 | 9 | 6 |
| HCN | 0.3 | 0.3 | 1.2 | 0.7 |
| Total[a/] | 31 | 35 | 60 | 63 |

a/ $H_2O$, $N_2$, $O_2$ free.

Table 3.- Gas from laser irradiation of macerals of Hernshaw (hvab) coal

| Maceral | $H_2$, percent[a/] | Volatile matter, percent[a/] | Product gas Moles x $10^7$ | Product gas $C_2H_2/CH_4$ |
|---|---|---|---|---|
| Fusinite | 3.2 | 13.4 | 43 | 59 |
| Micrinite | 4.8 | 31.4 | 52 | 34 |
| Vitrinite | 5.4 | 33.7 | 90 | 12 |
| Exinite | 6.4 | 55.4 | 103 | 8 |

a/ See reference 2.

Particle Size. Variation of gas yield with particle size was studied. Samples of Pittsburgh seam coal with particle diameters from 240 μ down to 10 μ (figure 1) were irradiated. For the smaller particles there was a modest decrease in methane and an increase in acetylene. This may indicate less cooling by conduction and higher temperatures.

Types of Lasers. Although laser activity has been produced in many different materials, this study has been carried out using only three--ruby, neodymium, and carbon dioxide. The ruby is a pink crystal of $Al_2O_3$ with 0.05 weight percent of $Cr_2O_3$. The chromium ions, excited by the xenon flash lamp, emit a pulse of 6,943 A laser light. The intensity of this pulse can be varied by changing the input to the lamp, by focusing the laser beam, and by Q-switching to shorten the discharge time. The standard irradiation for these experiments was a 6-joule pulse discharged in about 1 millisecond. Without optical alteration this produces a crater 6 mm in diameter (equal to the ruby rod) and an energy concentration at the target of 14 kw $cm^{-2}$. With a focusing lens this is increased to over 40 kw $cm^{-2}$ and, using an electro-optical Q-switch, to 40 Mw $cm^{-2}$.

The neodymium laser can deliver a 28-joule pulse of 10,600 A light. Using precise focusing but no Q-switching the light intensity at the target is about 400 kw $cm^{-2}$.

The $CO_2$ laser has a continuous output of 10 watts at a wavelength of 106,000 A. Using a focused beam it can produce a flux of 0.2 kw $cm^{-2}$.

Data from these three lasers, including several variations in the energy intensities of the ruby have been compared at approximately the same total energy output to determine if there are differences in product-gas quantity and distribution.

The $CO_2$ laser emits the least intense light beam because of its slow rate of emission. The ruby pulses were progressively increased in concentration due to focal variations. This can readily be measured on the coal targets. Craters in the coal irradiated by the defocused ruby laser beam had an average area of 1.3 $cm^2$. All irradiations with neodymium were focused and the craters averaged 0.02 $cm^2$. The best focused $CO_2$-laser beam produced a crater with an area of 0.03 $cm^2$. The product-gas data are shown as functions of crater area (figure 2). Only the data from irradiations with the $CO_2$ laser were not consistent with the other data due to its slow heating and cooling rates. The more intense laser beams produced greater quantities of product gas and higher acetylene to methane ratios. In figure 3 crater area was replaced by light flux (kilowatts $cm^{-2}$) and the $CO_2$-laser data could be included.

Temperature. Since the same amount of energy was available in each of these tests the temperatures of the craters or of the gas generating sites should be related to energy concentration. An attempt was made to estimate these temperatures from the composition of the gas using gas equilibria data. The chief interest is in the relationship between methane, acetylene, and hydrogen. Equilibrium data to 4,000 K are shown in figure 4.[4]

Gas analyses from various laser irradiations were introduced as shown in the sample calculation using data from irradiation with a neodymium laser.

$$K = \frac{(pC_2H_2)(pH_2)^3}{(pCH_4)^2} = \frac{(.00277)(.00987)^3}{(.000774)^2} = .00444$$

$$\log K = 2.351$$

Assuming the gases to be in equilibrium during their generation, figure 4 gives a temperature of 1,250° K. Temperatures were estimated for other laser irradiations where gas analyses were available (figure 5). Temperatures increase consistently with increase in energy concentration. Since acetylene was not detected in the gases from the $CO_2$ laser a temperature estimate could not be made. However, a gas analysis was available for product from a 900° C carbonization of coal and a comparison with equilibrium data indicated a temperature of 827° C, in reasonable agreement with the measured temperature.

Variations in types of irradiation cause great changes in gas yield and selectivity. However, most of these changes in the product can be explained on the basis of heat concentration at the target. A greater heat concentration increases gas yield, increases the probable crater temperature, and increases the acetylene to methane ratio. Even data from the $CO_2$ laser fits into this pattern although the heat concentration is achieved by additional radiation time instead of laser power.

Photochemistry. A fundamental question in the laser irradiation of coal is the possible importance of the wavelength of the energy. Is the laser simply a thermal energy source capable of raising coal to high temperatures or can the monochromatic energy stimulate specific chemical reactions in coal? The usual photochemical reactions take place with wavelengths of 2,000 A to 8,000 A.

The lasers available for this coal study were:

| | | |
|---|---|---|
| Ruby | 6,943 A | - visible spectrum |
| Neodymium | 10,600 A | - infrared |
| Carbon dioxide | 106,000 A | - infrared |

At this time it is impossible to measure the photochemical influence of the laser energy because duplicate craters have not been produced by different lasers and the temperature effect is much stronger than the photochemical effect. A first estimate is that the influence is small (compare ruby-focus and neodymium, figure 3) but perhaps using lower energy pulses differences can be detected.

Another conclusion to be drawn from these data is the effectiveness of a concentrated beam of laser light in promoting acetylene production in coal pyrolysis. This has been shown for both ruby and neodymium lasers and for coals of varying rank, maceral, and particle size. Due to coal volatility temperatures have been lower than expected. Higher coal temperatures could be predicted by irradiating pretreated coal in a pressurized system and should lead to gas compositions even richer in acetylene.

## References

1. Berkowitz, J., and Chupka, W. A., J. Chem. Phys., 40, 2735 (1964).

2. Ergun, S., McCartney, J. T., Mentser, M., Econ. Geology, 54, 1068 (1959).

3. Karn, F. S., Friedel, R. A., and Sharkey, A. G. Jr., Carbon, 5, 25 (1967).

4. McBride, B. J., Heimel, S., Ehlers, J. G., and Gordon, S., NASA SP-3001, Office of Sci. and Tech. Information, Nat'l Aeronautics and Space Admin., Washington, D. C., 1963, 328 pp.

5. Sharkey, A. G., Jr., Shultz, J. L., and Friedel, R. A., Bureau of Mines Report of Investigations 6868, 1966, 9 pp.

6. Shultz, J. L., and Sharkey, A. G. Jr., Carbon, 5, 57 (1967).

7. Verber, C. M., and Adelman, A. H., J. Applied Physics, 36, No. 5, 1522 (1965).

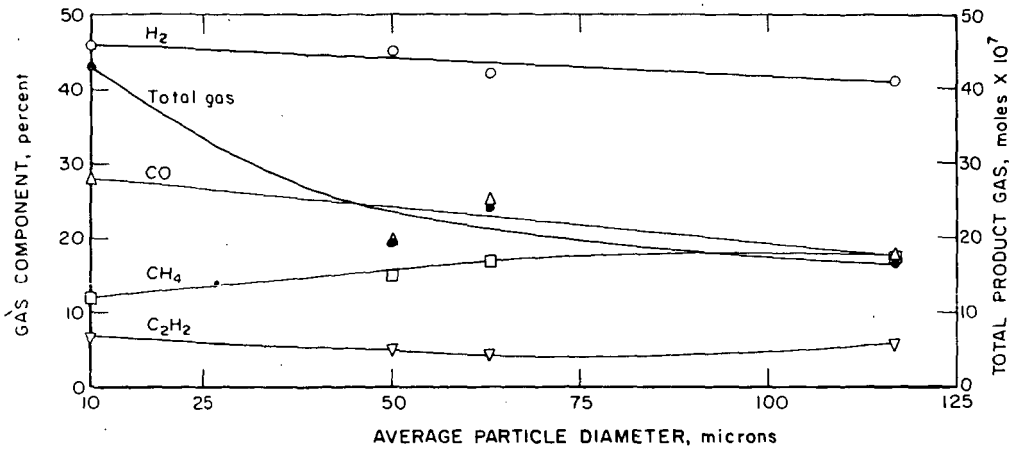


Figure 1. — Laser irradiation of Pittsburgh coal. Product gas as a function of coal particle diameter.

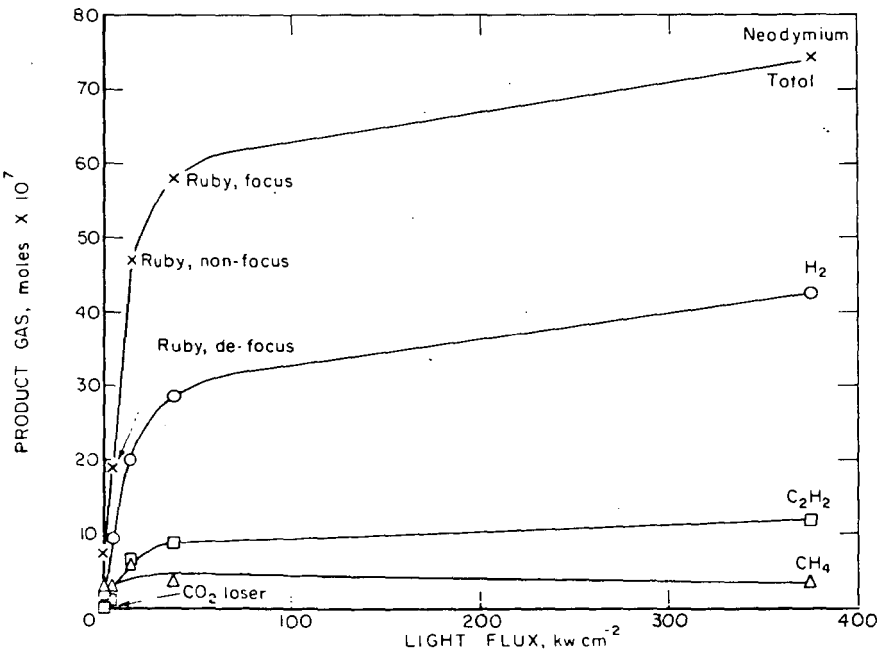


Figure 3 — Gas composition as a function of light flux. Laser irradiation of Pittsburgh seam coal.

L-10293

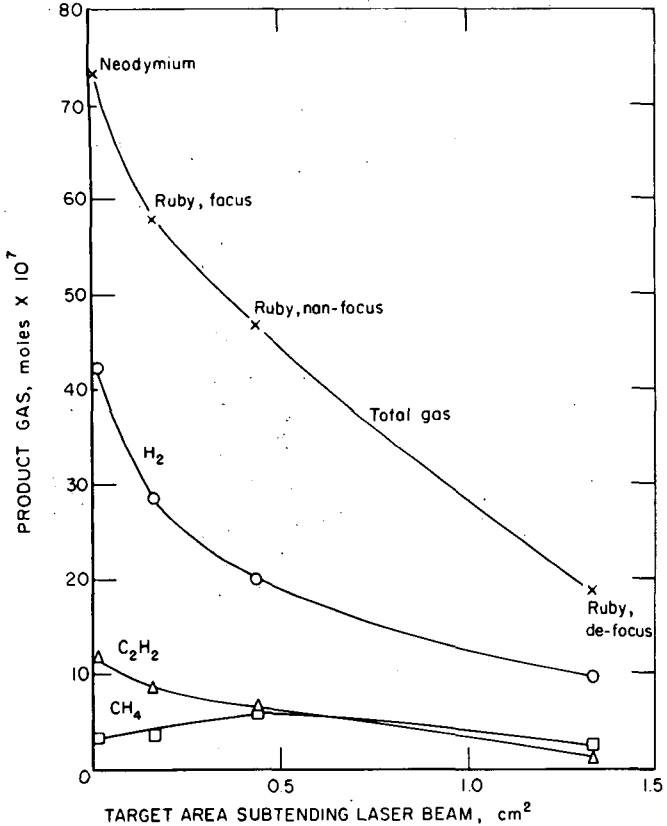


Figure 2.- Pittsburgh seam (hvab) coal irradiated with ruby and neodymium lasers. Gas in moles x $10^7$ per 6 joule pulse.

12-6-67 L-10292

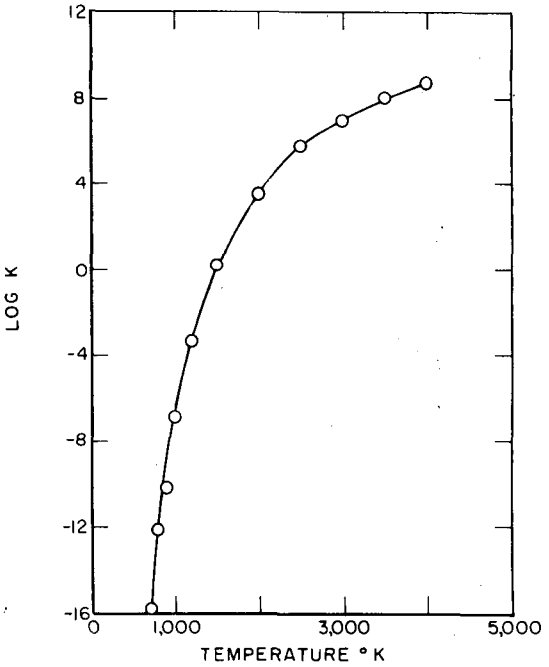


Figure 4.—Equilibrium for $2CH_4 \rightleftharpoons C_2H_2 + 3H_2$ calculated from NASA SP—3001. (ref 4)

L-10294

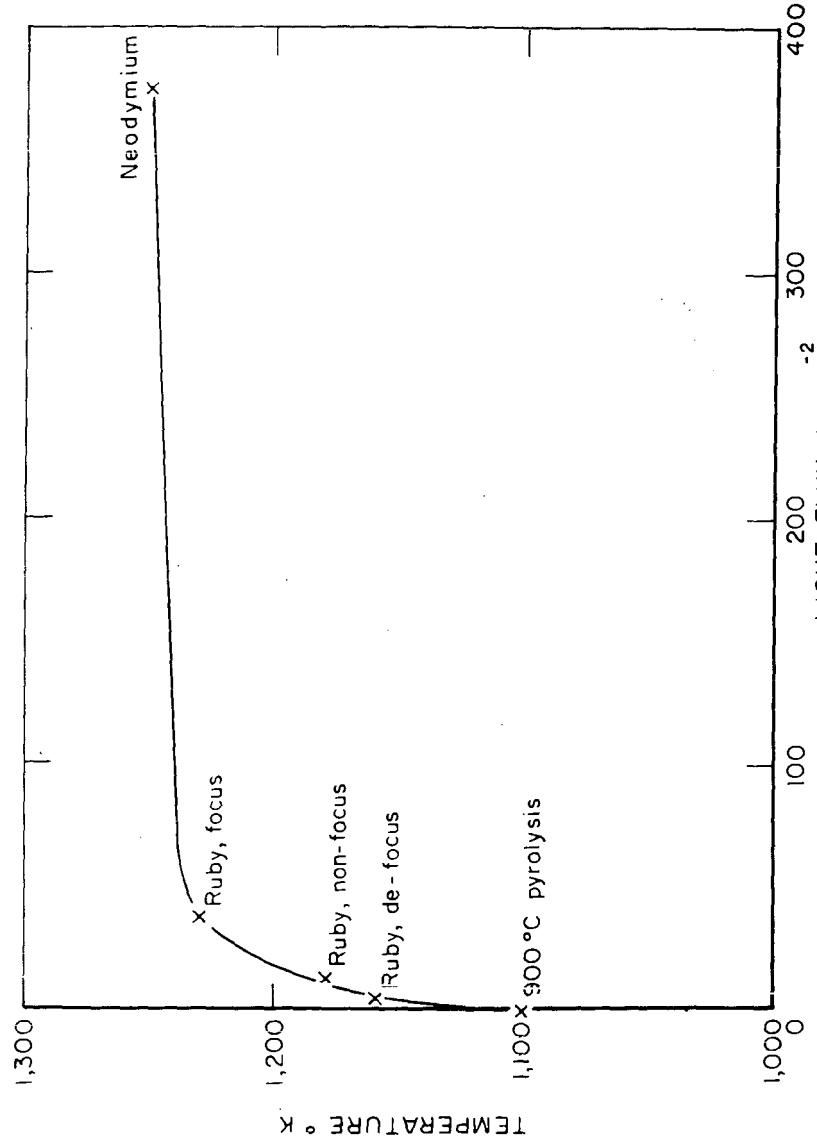


Figure 5.— Temperatures of laser irradiated coal as estimated from gas analyses.

# PYROLYSIS OF COAL IN A MICROWAVE DISCHARGE*

Yuan C. Fu and Bernard D. Blaustein

Pittsburgh Coal Research Center, Bureau of Mines,
U. S. Department of the Interior
4800 Forbes Avenue, Pittsburgh, Pennsylvania 15213

## INTRODUCTION

The nature of the thermal decomposition of coal differs greatly depending on the reaction temperature and the rate of heating. Recent investigations using various energy sources, e.g., plasma jets,[1-3] laser beam,[4,5] flash heating,[6] arc-image reactors,[7] etc., have shown that extremely rapid pyrolysis of coal produces high yields of acetylene. It has also been shown that high-volatile bituminous coal, when reacted in a microwave discharge in argon,[8] is readily gasified to produce a significant yield of acetylene.

The present study deals with the pyrolyses of coals of various ranks under the influence of a microwave discharge. The readiness of coal to give up a small part of its volatiles under the microwave irradiation permits the discharge to be sustained even when starting initially under a high vacuum. The relationship between the pressure increase during the discharge pyrolysis of coal and time shows that the principal reaction is a rapid gasification, which is induced by the active bombardment of the coal by energetic species present in the discharge. Studies of the gas composition at various stages of the discharge pyrolysis; of the effect of initial presence of Ar; and of the effect of cooling the gaseous products (as they are being formed); have all given further insight into the nature of the decomposition of coal which takes place in the microwave discharge.

## EXPERIMENTAL

Experiments were carried out in a Vycor tube reactor attached to a vacuum system provided with a Pace Engineering pressure transducer. The transducer was connected to a Fisher recorder, so that the pressure increase due to the devolatilization of coal in a known volume could be recorded during its discharge pyrolysis. The discharge was produced by a Raytheon microwave generator (2450 $MH_z$) coupled to an air-cooled Opthos coaxial cavity. The discharge was initiated by a Tesla coil either in a vacuum ( $\sim 10^{-4}$ mm Hg) or in the initial presence of argon (5-10 mm Hg), and the power level was maintained at 50 watts. The coal was located in the discharge zone.

All pressure-time data were obtained from experiments using 10 mg of vitrain of coal in a 163 ml reactor. Chemical analyses and origins of the vitrains of different coals used are given in Table 1. All the vitrains were -200 mesh, and were degassed in a high vacuum at 100° C prior to the experiment. The gaseous products were analyzed by mass spectrometry.

Tars and chars were pressed into KBr pellets for infrared analysis. Tars were also dissolved in benzene or ethanol for ultraviolet analysis.

---

* Vitrains of coals were used throughout this paper.

Table 1. Analyses of vitrains (moisture free basis, percent)

| | C | H | N | S | O (by diff.) | Ash | Volatile matter |
|---|---|---|---|---|---|---|---|
| Anthracite[1/] | 91.06 | 2.49 | 0.96 | 0.83 | 2.98 | 1.77 | 6.1 |
| Low volatile bituminous[2/] | 89.57 | 4.67 | 1.25 | .81 | 2.17 | 1.53 | 20.2 |
| High-volatile bituminous[3/] | 81.77 | 5.56 | 1.71 | .97 | 7.93 | 2.06 | 39.2 |
| Lignite[4/] | 66.45 | 5.40 | .31 | 1.40 | 22.84 | 3.60 | 44.0 |

1/ Dorrance Mine, Lehigh Valley Coal Co., Luzerne County, Pennsylvania.
2/ Pocahontas No. 3 Bed, Buckeye No. 3 Mine, Page Coal and Coke Co., Stephenson, Wyoming County, West Virginia.
3/ Bruceton, Pennsylvania Bed, Allegheny County, Pennsylvania.
4/ Beulah-Zap Bed, North Unit, Beulah Mine, Knife River Coal Mining Co., Beulah, Mercer County, North Dakota.

## RESULTS AND DISCUSSION

### Gas Evolution During the Discharge Pyrolysis

Coal, on being subjected to microwave radiation and excitation by a Tesla coil, readily gives up enough of its volatiles to sustain the discharge initially. Figure 1 shows the pressure-time relationships during the discharge pyrolyses for a lignite, a high-volatile bituminous coal, a low-volatile bituminous coal, and an anthracite. The zero time is the time the plasma appeared, and there is usually some sort of "induction period" before an extensive build-up of the pressure takes place, except for the lignite where the pressure rise is spontaneous. For each vitrain, the pressure reaches a plateau after some time. Substantial amounts of tars were produced from the hvab and the lvb coals, and it was noticed that the tars deposited on the reactor wall immediately after the discharge was initiated.

The results and the pressure-time relationships show that the discharge pyrolysis of coal (except for lignite) may be divided into three stages:

(1) Partial carbonization to produce tar. This proceeds at a relatively low rate without significant gas evolution -- an "induction period" for gas evolution.

(2) The principal reaction -- pyrolysis with accompanying gasification. This proceeds at a relatively high rate.

(3) Degassing of residual char. This rate is very slow.

The high evolution of gases in the second stage takes place only after the pressure in the system has gradually built up to a point (0.5 to 1 mm), where there are sufficient concentrations of electrons, atoms, and ions present in the discharge so that these energetic species can actively bombard the coal to accelerate the decomposition of the coal. For the lignite the rapid gas evolution takes place spontaneously, presumably owing to its readiness to release sufficient amounts of volatile matter which is converted to the energetic species. As shown in Figure 1, the rate of gas evolution at this stage increases with volatile matter content of the coal.

In the third stage, the gas evolution reaches a limit. Table 2 shows the typical product analyses obtained at the end of the reaction time indicated in Figure 1. The extent of devolatilization or gasification increases with volatile matter content of the coal. In general, the amounts of gases evolved are comparable to those evolved from thermal decompositions of the coals at about 1000° C, but the products are richer in $H_2$ and $C_2H_2$.

Table 2. Discharge pyrolysis of coal

| | Lignite | hvab | lvb | Anthracite |
|---|---|---|---|---|
| Volatile matter, percent | 44.0 | 39.2 | 20.2 | 6.1 |
| Reaction time, min | 10 | 20 | 20 | 20 |
| Product, $10^{-1}$ mmoles/g. coal | | | | |
| $H_2$ | 86.5 | 103 | 120 | 60.2 |
| $CH_4$ | 2.7 | 3.5 | 1.4 | 5.0 |
| $C_2H_2$ | 7.8 | 15.0 | 7.9 | 1.8 |
| $C_2H_6$ | 0.7 | 0.9 | 0.2 | trace |
| CO | 83.5 | 35.7 | 11.3 | 3.9 |
| $CO_2$ | 8.7 | 0.8 | 0.1 | trace |
| $H_2O$ | 5.5 | 2.0 | 3.5 | 1.9 |
| Total gases, wt pct | 32.6 | 17.5 | 8.6 | 3.3 |
| C gasified, percent | 20.6 | 11.1 | 4.2 | 1.2 |
| C converted to gaseous hydrocarbons, percent | 3.9 | 5.7 | 2.7 | 0.6 |

## Effect of Initial Presence of Argon

The pressure-time relationship during the discharge pyrolysis in the presence of added argon (Figure 2) shows that the rapid gas evolution takes place as soon as the discharge is initiated and proceeds at a higher rate. Here, the gas evolution also quickly reaches a limit, but the initial "induction period" for the gas evolution does not exist. Evidently, the added argon immediately forms sufficient concentrations of energetic species upon initiation of the discharge, thus allowing stages 1 and 2 to proceed concurrently. The gas evolution reaches a limit sooner, but the extent of devolatilization of the coal and the gaseous product type do not differ significantly. The results are shown in Table 3.

## Gas Composition at Various Stages of Discharge Pyrolysis

In order to investigate the composition of the gases evolved at various stages of the devolatilization, the pyrolysis was interrupted at several stages by discontinuing the discharge. At each stage, the evolved gases were measured and collected for mass spectrometric analysis. The discharge -- and the pyrolysis -- were then continued for the remaining coal until no more noticeable devolatilization could be observed.

Figures 3 and 4 show the results obtained for the lignite and the hvab coal, respectively. The gas composition at various stages of the thermal pyrolysis (the gases were collected at 200° C interval) of the hvab coal is also shown in Figure 5 for comparison. Acetylene in addition to methane are the major constituents of the hydrocarbons produced from the discharge pyrolysis, and their concentrations are nearly constant at each stage, except that they decrease at the later stages, possibly because of less evolution of hydrogenated carbon-species from the coal.

Table 3. Discharge pyrolysis of coal in the presence of Ar

| | Lignite | hvab | lvb | Anthracite |
|---|---|---|---|---|
| Volatile matter, percent | 44.0 | 39.2 | 20.2 | 6.1 |
| Initial pressure of Ar, mm | 5.1 | 5.1 | 5.1 | 5.1 |
| Reaction time, min | 5 | 20 | 20 | 20 |
| Product, $10^{-1}$ mmoles/g. coal | | | | |
| $H_2$ | 86.8 | 98.5 | 113 | 64.5 |
| $CH_4$ | 2.1 | 2.5 | 4.0 | 0.4 |
| $C_2H_2$ | 10.4 | 15.8 | 8.8 | 2.0 |
| $C_2H_4$ | 0.6 | 0.7 | 0.8 | trace |
| CO | 79.5 | 31.9 | 10.8 | 4.2 |
| $CO_2$ | 8.6 | 0.7 | 0.2 | trace |
| $H_2O$ | 7.5 | 3.4 | 4.9 | 1.6 |
| Total gases, wt pct | 33.5 | 16.5 | 9.4 | 3.4 |
| C gasified, percent | 19.4 | 11.4 | 4.9 | 1.2 |
| C converted to gaseous hydrocarbons, percent | 4.5 | 6.6 | 3.5 | 0.7 |

Tar -- Substantial amounts of tars were obtained from the hvab and the lvb coals in the discharge pyrolyses. The tars were compared by IR and UV analyses with the tar obtained from the thermal pyrolysis (at 700° C) of the hvab coal. All the IR spectra showed the presence of usual aliphatic C-H bands (2860-2940 $cm^{-1}$) and aromatic bands (740-860 $cm^{-1}$) which are typical of pitch and coal. The tars obtained from the discharge pyrolyses, however, exhibited weaker aromatic bands and a stronger carbonyl band (1710 $cm^{-1}$) than the tar obtained from thermal pyrolysis. The UV spectra (of the tars extracted by benzene or ethanol) exhibited no distinct absorption band for the tar obtained from the thermal pyrolysis, but exhibited bands at 3140, 3300, and 3470 Å (which could be attributed to derivatives of pyrene) for those obtained from the discharge pyrolyses.

All the residual chars exhibited no distinct band over the entire IR spectrum.

Effect of Cooling by Liquid Nitrogen

A. Hvab Coal -- When one end of an h-shaped reactor (vol. = 41 ml) was cooled with liquid $N_2$ while the other leg containing the hvab coal was subjected to the discharge pyrolysis, it was observed that the pressure reading of the reactor never exceeded 0.5 mm during the course of the decomposition. The end products consisted mainly of hydrocarbons and water, without significant amounts of $H_2$ and CO. Acetylene was the main hydrocarbon, but substantial amounts of other $C_2$, $C_3$, $C_4$, $C_5$ and $C_6$ hydrocarbons were also formed. Without liquid $N_2$ cooling, the other $C_2$ and $C_3$ hydrocarbons were insignificant and the $C_4$, $C_5$ and $C_6$ hydrocarbons were not measurable. The product analyses, except that for $C_4$, $C_5$ and $C_6$ hydrocarbons which constitute less than 2 percent of the gases, are shown in Table 4. The extent of devolatilization and the hydrocarbon yield are significantly increased.

Table 4. Effect of liquid nitrogen cooling on discharge pyrolysis of coal

| | $P_{Ar}$ mm | Time, min. | Product, $10^{-1}$ mmole/g. coal | | | | | | | | | Total gases, wt percent | Percentage of C present as | |
|---|---|---|---|---|---|---|---|---|---|---|---|---|---|---|
| | | | $H_2$ | $CH_4$ | $C_2H_2$ | $C_2H_4$ | $C_2H_6$ | $C_3H_6$ | $C_3H_8$ | CO | $CO_2$ | $H_2O$[2] | | Gaseous products | Gaseous hydrocarbons |
| hvab [1] | - | 15 | 1.2 | 0.4 | 40.4 | 3.4 | 5.6 | 2.9 | 1.7 | 2.7 | 0.8 | 23 | 20.4 | 17.2 | 16.7 |
| [1] | - | 30 | 3.2 | 0.5 | 48.4 | 3.6 | 9.4 | 3.8 | 2.7 | 3.6 | 0.7 | 30 | 26.2 | 21.7 | 21.1 |
| [1] | - | 45 | 1.1 | 0.4 | 48.8 | 2.6 | 7.5 | 4.5 | 3.0 | 4.5 | 0.7 | 26 | 25.3 | 21.6 | 20.8 |
| | 10 | 30 | 17.6 | 0.4 | 85.2 | 6.1 | 5.4 | 0.9 | 0.7 | 6.7 | 1.3 | 14 | 31.7 | 30.4 | 29.3 |
| Lignite | - | 7 | 0.6 | 0.5 | 47.0 | 1.9 | 3.7 | 0.7 | 0.9 | 0.8 | 13.8 | 74 | 34.3 | 22.7 | 20.1 |
| | - | 10 | 0.9 | 0.3 | 50.2 | 1.0 | 3.2 | 0.6 | 1.0 | 0.6 | 11.9 | 75 | 34.0 | 22.8 | 20.6 |
| | 10 | 20 | 12.9 | 0.2 | 38.2 | 0.8 | 1.3 | 0.3 | 0.3 | 9.8 | 14.2 | 43 | 27.8 | 19.3 | 14.9 |

[1] $C_4$, $C_5$, and $C_6$ hydrocarbons were also formed.

[2] $H_2O$ content as obtained from mass spectrometric analyses are only approximate, and data are reported only to show trends.

With Ar initially present and with cooling, however, the pressure reading increased rather rapidly to a maximum within a few minutes, and then decreased gradually. Presumably, large amounts of $H_2$, CO (noncondensable at -196° C) and hydrocarbons were rapidly formed due to the high rate of gasification of the coal in the Ar discharge. The pressure decrease in the later stage is attributed to the continuous reaction of $H_2$ and CO to form condensable hydrocarbons. As seen in Table 4, however, appreciable $H_2$ and CO still remained after 30 minutes of reaction. The yield of acetylene is very high, but that of other $C_2$ and $C_3$ hydrocarbons is low. No measurable amounts of $C_4$, $C_5$ and $C_6$ hydrocarbons were found

These results may be interpreted as follows. In the absence of added Ar, small reactive species (H, O, C, CH, etc.) and perhaps some larger fragments (radicals) are slowly detached from coal molecules, but are rapidly converted to stable products such as acetylene, higher hydrocarbons, and water, which are finally condensed at the liquid $N_2$ temperature. In the presence of Ar, however, the detachment of these fragments proceeds at such a high rate that all the products formed cannot be immediately condensed by the liquid $N_2$. As a result, the larger molecules further decompose or react with O-species to form large amounts of $H_2$ and CO. It is also quite possible that different types of species (or smaller fragments) are released in the presence of Ar, resulting in rapid formation of noncondensable $H_2$ and CO. With prolonged reaction time, the $H_2$ and the CO would then continue to react to form relatively lower hydrocarbons and water.

Increases in the extent of devolatilization and in the hydrocarbon yield under these conditions are due primarily to the removal of hydrocarbons (therefore no further decomposition or polymerization), and of water[9] (therefore no reaction of water with hydrocarbons to form $H_2$ and CO).

B. Lignite -- As seen in Figure 1, lignite releases gases spontaneously at a higher rate than the hvab coal. Thus, when the discharge pyrolysis of the lignite was subjected to liquid $N_2$ cooling, it was observed that the pressure reading increased rapidly to a maximum within 1 to 2 minutes, and then decreased gradually to practically zero after several minutes. At this point, the major part of the pyrolysis of the coal seemed to be completed and the discharge could not be maintained.

The reasons for this different behavior (from that of the hvab coal) may be (i) the spontaneous gas evolution at a higher rate and (ii) the release of more numerous smaller fragments from lignite, resulting in rapid formation of noncondensable $H_2$ and CO. All the $H_2$ and the CO are eventually converted to hydrocarbons and water in the later stage. The results in Table 4 also show that the hydrocarbon yield is very significantly increased under these conditions.

Similar behavior was observed with added Ar except that some part of the $H_2$ and CO remain unreacted, owing perhaps to the slowness with which the product species diffusing into the cold trap in the presence of high concentration of Ar.

It was also noticed that the lignite yielded a significant amount of $CO_2$, while the hvab coal yielded very small amounts of $CO_2$ under all conditions. This suggests that $CO_2$ molecules are released from the lignite structure rather than formed from interactions of CO and active O-species in the discharge.

## CONCLUSIONS

The principal reaction in the discharge pyrolysis of coal is rupture of the bonds in the coal structure by bombardment of energetic species (whether released from the coal or formed from argon in the discharge) on the coal surface. Numerous species such as H-species, O-species, gaseous C, and hydrogenated carbon fragments (CH, $C_2H$ or $C_xH_y$) are produced from coal in the discharge, these in turn decompose or combine with each other to form hydrogen, water, carbon oxides, and hydrocarbons. After extensive decomposition of the coal structure, all the species present in the discharge reach a steady state, where the formation of hydrocarbons is limited by back reactions with water to form $H_2$ + CO and gasification of solid is somewhat compensated by polymerization of hydrocarbons.

Thus, if the decomposition products are rapidly removed by a liquid nitrogen trap as they are formed, high yield of hydrocarbons consisting mainly of acetylene can be obtained. The process for the discharge pyrolysis of high-volatile bituminous coal under these conditions is unique in that it converts more than 21 percent of carbon in coal to higher hydrocarbons (up to $C_6$) without the accompanying formation of $H_2$ and CO. With argon initially present under similar conditions, however, the pyrolysis products are lower hydrocarbons (below $C_4$) and substantial amounts of $H_2$ and CO, owing to the increased rate of gasification. Hence, the product type and distribution can be influenced by the rate of formation or removal of the products.

## ACKNOWLEDGEMENTS

The authors wish to thank Dr. Irving Wender for his valuable discussions, Gus Pantages and George Kambic for their technical assistance, A. G. Sharkey, Jr. and Janet L. Shultz for their mass spectrometric analyses, and John Queiser for his infrared analysis.

## REFERENCES

1. Bond, R. L., Ladner, W. R., and McConnell, G. I. T. Fuel, Lond. 1966, 45, 381
2. Graves, R. D., Kawa, W., and Hiteshue, R. W. Ind. Eng. Chem. Proc. Design and Develop., 1966, 5, 59
3. Kawana, Y., Makino, M., and Kimura, T. Kogyo Kagaku Zasshi, 1966, 69, 1144
4. Shultz, J. L. and Sharkey, A. G. Jr. Carbon, 1967, 5, 57
5. Karn, F. S., Friedel, R. A., and Sharkey, A. G. Jr. Carbon, 1967, 5, 25
6. Rau, E. and Seglin, L. Fuel, Lond. 1964, 43, 147
7. Rau, E. and Eddinger, R. T. Fuel, Lond. 1964, 43, 246
8. Fu, Y. C. and Blaustein, B. D. Chem. and Ind., Lond. 1967, 1257.
9. Blaustein, B. D. and Fu, Y. C. In "Chemical Reactions in Electrical Discharges," Adv. Chem. Series, R. F. Gould, Editor, Amer. Chem. Soc., Washington, D. C., Volume in press, 1968

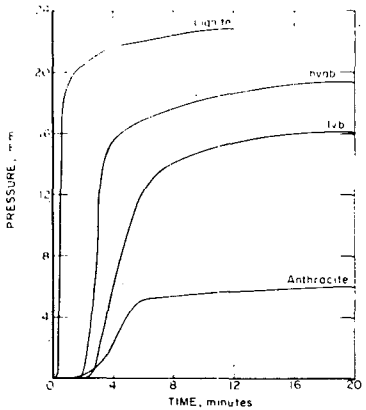


Figure 1 — Pressure as a function of time during the discharge pyrolysis of coal (10 mg coal in 163 ml reactor)

12-12-67 L-10305

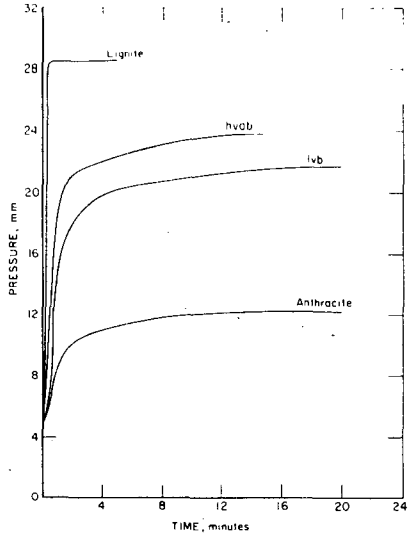


*Figure 2 - Pressure as a function of time during the discharge pyrolysis of coal in the presence of Ar ($P_{Ar}$ = 51 mm, 10 mg coal in 163 ml reactor)*

12-5-67 L-10288

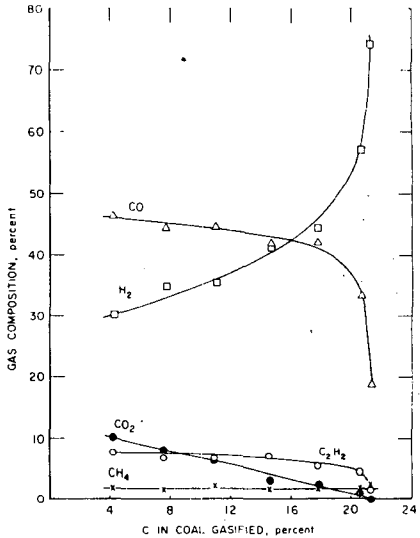


Figure 3 - Gas composition at various stages of discharge pyrolysis of lignite.

12-5-67 L-10289

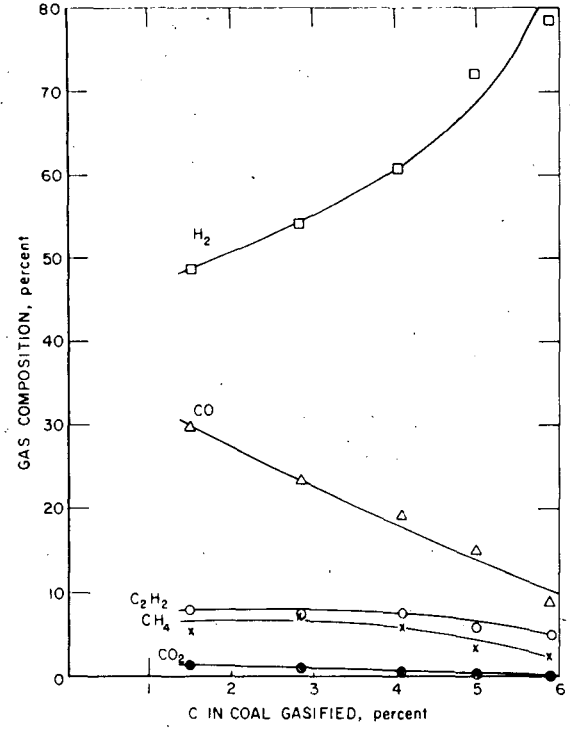


Figure 4.- Gas composition at various stages of discharge pyrolysis of hvab coal.

12-5-67 L-10290

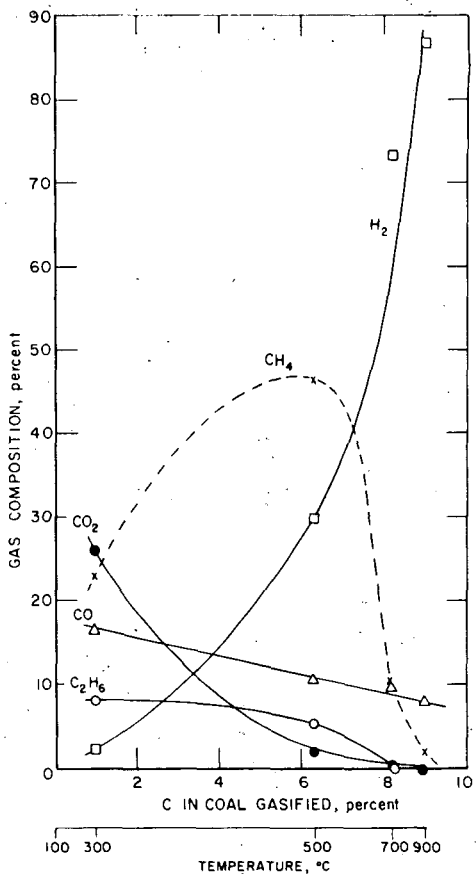


Figure 5.- Gas composition at various stages of thermal pyrolysis of hvab coal.

12-5-67 L-10291

# KINETICS OF HYDROCRACKING OF LOW TEMPERATURE COAL TAR

S. A. Qader, W. H. Wiser, and G. R. Hill

Department of Fuels Engineering,
University of Utah,
Salt Lake City, Utah

## Abstract

The results of hydrocracking of a low temperature coal tar in a batch autoclave over a catalyst containing sulphides of nickel and tungsten, supported on silica-alumina, indicated that gasoline can be obtained in a yield of 77% at 500°C and 3000 psi pressure. The highest quality product, containing 60% aromatics and 13% isoparaffins, was obtained at 450°C and 2000 psi but in a lower yield of 60%. Most of the sulfur, nitrogen, and oxygen present in the tar were removed. The gasoline formation, desulphurization, and denitrogenation reactions were all found to be of first-order with activation energies of 17,000, 14,500, and 15,000 calories per mole respectively. Linear relationships were found between rate constants for gasoline formation ($k_g$), desulphurization ($k_s$) and denitrogenation ($k_n$) as can be represented by the following equations:

$$k_g = 1.1371\ k_s - 0.1278$$

$$k_g = 2.11\ k_n - 0.0669$$

$$k_n = 0.5397\ k_s - 0.0837$$

Hydrocracking reactions involving the breakage of chemical bonds on the catalyst surface are rate-determining.

## Introduction

Hydrocracking has been investigated in recent years as a potential method for upgrading coal-derived liquids. The work reported so far is very much limited and the fundamental aspects of such processing are not well understood. Much of the earlier work was carried out in connection with the coal hydrogenation processes (Gordon, 1935, 1940, and 1947 and Pier, 1949) where a two-stage reaction was used in which the first stage liquified the coal and the second converted the resulting heavy distillates to gasoline by catalytic hydrocracking. Carpenter, et al (1963) reported the results of hydrocracking a lignite tar in a continuous fixed bed reactor over cobalt-molybdate and zinc chromite catalysts for producing gasoline. A maximum yield of 59% of gasoline was obtained at 477°C and 3000 psi pressure. Rutkowski

(1965) studied the influence of temperature, pressure, hydrogen-oil ratio, diluents, and catalysts on the hydrocracking of low temperature tars and reported minimum coke yields using tetralin and cyclohexane as diluents. Katsobashvili and Elbert (1966) reported a yield of 83.8% saleable products when a tar distillate boiling from 230° to 360°C was hydrocracked in a continuous fixed bed reactor at 500° to 550°C and 50 atmospheres under recycle conditions. The economic feasibility of producing gasoline from coal by the H-coal process, wherein the heavy oil produced in the first stage was hydrocracked in a subsequent stage, was demonstrated by the results published by Alpert, et al (1966). Zielke, et al (1966) investigated the suitability of zinc halide catalysts for hydrocracking coal extracts for the production of gasoline. The results indicated that a maximum yield of 68% of gasoline could be obtained at 427°C, 4200 psi pressure and 60 minutes reaction time. In the present communication, the results of hydrocracking of a low temperature coal tar in a batch autoclave over a catalyst containing sulphides of nickel and tungsten, supported on silica-alumina, are described. The influence of temperature and pressure on product distribution and kinetic evaluation of the data are presented.

## Experimental

### Materials.

Low temperature tar from a high volatile bituminous coal from Utah was prepared by carbonization at 550°C in a laboratory oven. The light oil boiling up to 200°C was separated from tar by distillation (Table I). The catalyst (commercial) contained 6% nickel and 19% tungsten, both as sulphides, supported on silica-alumina and had a surface area of 212 sq. meters per gram and size of -200 mesh. 5-A molecular sieves were of chromatographic grade.

### Equipment.

A 1-litre high pressure autoclave with a magnetic drive stirrer, pressure and temperature control devices, liquid and gas sampling lines, and water quenching system (Figure 1) and hydrogen cylinders with maximum pressure of 2300 psi were used.

### Procedure for hydrocracking experiments.

In each experiment 100 c.c of tar and 10 grams of the catalyst were used. The equipment was evacuated to remove most of the air, filled with hydrogen and heated to the desired temperature. The temperature rose to 300°C in 21 minutes and 500°C in 28 minutes. The reaction time was taken from the start of heating the equipment. When the reaction temperature was reached, the pressure was adjusted to the experimental value and maintained constant throughout except in experiments conducted at pressures higher than 2000 psi where there was a reduction in pressure of about 200 to 300 psi during

the course of the experiment. Experiments were conducted at different reaction times and 4 gas samples were taken out during each experiment. At the end of the reaction time, heating was stopped and the product was quenched rapidly by circulating water in the cooling coil immersed in it. It took 1 to 2 minutes to cool the product down to 250°C and 15 minutes to atmospheric temperature. The pressure was then released slowly and the autoclave opened. The product was transferred to a beaker, filtered to remove the catalyst, and the water separated to get the total oil product. The mechanical losses were found to be less than 1%. The yield of the product was taken as 100% and 100 minus the volume of the total oil product was taken as percent conversion to gas. A few c.c of the total oil product were used for sulfur and nitrogen analysis and the remainder was washed with 10% sodium hydroxide and 20% sulphuric acid to remove tar acids and bases respectively. The neutral oil was then distilled into a gasoline fraction boiling up to 200°C, a diesel oil fraction boiling from 200° to 360°C and residue. The volume of each fraction in c c obtained from the total oil product was taken as volume percent conversion to that particular fraction

Product analysis.

Sulfur was determined by the bomb method and nitrogen by the C-H-N chromatographic analyzer, F.M. Model 185. Tar acids and bases were estimated by extraction with 10% sodium hydroxide and 20% sulphuric acid respectively. Hydrocarbon-type analysis was done by the Fluorescent-Indicator-Adsoprtion method (ASTM, D1319-65T). For the estimation of naphthenes and isoparaffins, the saturated hydrocarbon portion was first separated from the mixture by sulphonation with a mixture of 70% concentrated sulphuric acid and 30% phosphorus pentoxide (ASTM, D1019-62). The naphthenes were estimated by the refractivity intercept method (ASTM, D1840-64). The N-paraffin content was determined by adsorption over 5-A molecular sieves in a glass column of 0.5-inch diameter and 1.5-foot length. The isoparaffins were obtained by the difference. The diesel index was calculated from API gravity and aniline point. The gas analysis was done by gas chromatography in the F.M. Model 720 dual column programmed temperature gas chromatograph.

Results and Discussion

Product distribution.

The yield of gasoline and gas and the iso-normal ratio in butanes increased with temperature whereas the diesel oil decreased while the residue remained almost the same (Figure 2). Tar acids and bases were removed completely along with most of the sulfur and nitrogen at 450°C and 1500 psi pressure (Table II). Isomerization increases with cracking and the gas yield and iso-normal ratio in butanes are qualitative indications of the extent of cracking reactions taking place leading to the formation of gasoline. A

pressure of 1500 psi is sufficient to suppress coke-forming reactions and the gasoline is formed mainly by the cracking of the diesel oil, thereby affecting the quantity and quality of the latter. The composition of gasoline obtained at different temperatures remains almost the same and the aromatics of the gasoline are mainly formed by the dealkylation of alkylbenzenes, hydrocracking of hydro-aromatics, and hydroremoval of sulfur, oxygen, and nitrogen compounds.

The gasoline yield increased at different rates with pressure (Figure 3). The rate of gasoline formation was high in the pressure range 1000 to 1500 psi, slowing down in the range 1500 to 2500 psi, and increasing again at higher pressures. The residue decreased rapidly in the range 1000 to 1500 psi but the decrease was small at higher pressures. On the other hand, the gas yield and iso-normal ratio in butanes remained almost constant up to a pressure of 1500 psi and increased at higher pressures (Figure 4). Pressure does not have a marked influence on cracking reactions in the range 1000 to 1500 psi but the increase in the yield of gasoline is due to the suppression of the coke-forming reactions. In the range 2000 to 2500 psi, partial hydrogenation of aromatics to hydro-aromatics takes place followed by the cracking of the latter which increases the yield of gasoline and the aromatic content (Figures 5 to 7). At higher pressures complete hydrogenation of aromatics to naphthenes takes place and increases the gasoline yield. The naphthenes in the gasoline increase with a corresponding decrease in the aromatics. Isomerization increases with pressure and temperature. High aromatic gasolines were obtained in the pressure range 1750 to 2500 psi (Table III). A maximum yield of 77% of gasoline was obtained at 500°C and 3000 psi pressure but the highest quality product containing 60% aromatics and 13% isoparaffins was formed at 450°C and 2000 psi pressure which can compare well with the premium grade gasoline from petroleum (Table IV).

Kinetics

Equilibrium was reached at different time periods at different temperatures with respect to gasoline formation but the conversion was 100% in the case of sulfur and nitrogen removal (Figures 8 to 10). The sulfur and nitrogen removal reactions are not governed by thermodynamic limitations but are limited only by kinetic factors under the experimental conditions employed. Plots of $\log \frac{a}{a-x}$ versus time (Figures 11 to 13), where "a" is the equilibrium conversion in case of gasoline and initial concentration in case of sulfur and nitrogen, are linear and the hydrocracking reactions with respect to gasoline formation and removal of sulfur and nitrogen are all first-order. The first-order rate constants are thus represented by equations 1 to 3.

$$\frac{d\,(\text{Gasoline})}{dt} = k_g\,(\text{Tar}) \qquad (1)$$

$$-\frac{d\,(\text{Sulfur})}{dt} = k_s\,(\text{Sulfur}) \qquad (2)$$

$$-\frac{d\,(\text{Nitrogen})}{dt} = k_n\,(\text{Nitrogen}) \qquad (3)$$

where "kg," "$k_s$," and "$k_n$" are rate constants for gasoline formation and removal of sulfur and nitrogen respectively. There was no change in the concentration of hydrogen in the system during the course of the reaction since the hydrogen pressure was maintained constant throughout. Hydrogen atoms may be involved in the rate-determining step but their concentration constitutes one of the constant factors in the rate constant term and does not show up in the rate equation. However, hydrogen actually takes part in the hydrocracking reactions and, hence, the reactions are considered pseudo-first-order

The hydrocracking reactions under study follow true Arrhenius temperature dependence (Figure 14) and the rate constants can be represented by equations 4 to 6.

$$k_g = 0.1567 \times 10^6\, e^{-17,600/RT} \text{ hrs.}^{-1} \qquad (4)$$

$$k_s = 0.2134 \times 10^5\, e^{-14,500/RT} \text{ hrs.}^{-1} \qquad (5)$$

$$k_n = 0.4738 \times 10^5\, e^{-15,900/RT} \text{ hrs.}^{-1} \qquad (6)$$

The following values of enthalpies and entropies of activation were calculated by the Eyring equation plotting log k'/T versus $\frac{1}{T}$ (Figure 15).

$$\Delta H_g = 16,200 \text{ cal /mole}, \quad \Delta S_g = -43.5 \text{ e.u.}$$

$$\Delta H_s = 12,200 \text{ cal /mole}, \quad \Delta S_s = -44.9 \text{ e.u.}$$

$$\Delta H_n = 14,900 \text{ cal /mole}, \quad \Delta S_n = -45.9 \text{ e.u.}$$

Linear relationship was found between $k_g$, $k_s$, and $k_n$ (Figure 16) and can be represented by equations 7 to 9

$$k_g = 1.1371\, k_s - 0.1278 \qquad (7)$$

$$k_s = 2.1100\, k_n - 0.0669 \qquad (8)$$

$$k_n = 0.5397\, k_s - 0.0837 \qquad (9)$$

A major part of the gasoline is expected to be formed by the cracking of hydrocarbons, but a minor part comes from the decomposition of some of the sulfur, oxygen, and nitrogen compounds. The yield of gasoline thus depends, to some extent, on the removal of sulfur and nitrogen and this may result in some sort of interrelationship between $k_g$, $k_s$, and $k_n$. The dissociation energies of the C-C, C-S, and C-N bonds may also have some influence on the above relationship, especially between $k_s$ and $k_n$. However, the results presented in this paper do not throw much light on the effect of other temperature and pressure conditions and equations 7 to 9 are not considered to be having much quantitative significance at this stage.

The energies and enthalpies of activation indicate that chemical reactions but not physical processes are rate-controlling. The probable chemical reactions occurring during hydrocracking are cracking, isomerization, hydrogenation, polymerization, condensation, and dehydrogenation, all taking place on the catalyst surface. Under the experimental conditions employed, polymerization, condensation, and dehydrogenation are very much suppressed and may be eliminated. It has been established by Weisz and Prater (1957) and Keulemans and Voge (1959) that reactions occurring on acidic sites of the dual-functional catalyst, like the one used in this investigation, are rate-determining which eliminates the possibility of hydrogenation reactions to be rate-limiting. Hence, cracking reactions involving the breakage of chemical bonds and the isomerization reactions, wherein skeletal rearrangement of carbonium ions takes place, must be rate-limiting. It is known that in catalytic hydrocracking, cracking precedes isomerization and only the isomerization of the cracked fragments occurs without any change of the uncracked material (Flinn, et al., 1960, and Archibald, et al., 1960). An excess of branched isomers than can be predicted by thermodynamic equilibrium are also formed; the latter can only happen if the isomerization of the cracked fragments can occur very rapidly and leave the catalyst surface without appreciable readsorption. Therefore, the isomerization is believed to be very rapid and cannot be rate-controlling. Hence, the cracking reactions, involving the breakage of chemical bonds on the catalyst surface, are rate-determining.

Acknowledgment

The research work reported in this paper was sponsored by the U. S. Office of Coal Research and the University of Utah.

Table I. Properties of Feed Material

| | |
|---|---|
| Sp. gr. (25°C) | 0.9942 |
| Tar acids, vol. % of feed | 30.0 |
| Tar bases, wt. % of feed | 3.5 |
| Sulfur, wt. % of feed | 0.6984 |
| Nitrogen, wt. % of feed | 0.4018 |
| Distillation data | |
| I.B.P., °C. | 200 |
| 50% distillate | 298°C |
| Pitch point | 360°C |
| Residue, vol. % of feed | 30.0 |
| Hydrocarbon types in neutral fraction 200° to 360°C, vol. % | |
| Saturates | 32.0 |
| Olefins | 19.0 |
| Aromatics | 49.0 |

Table II. Influence of Temperature on Product Distribution (Pressure, 1500 psi)

| Temp. (°C.) | 400 | 425 | 450 | 475 | 500 |
|---|---|---|---|---|---|
| Reaction Time, hrs. | 13 | 12 | 10 | 8 | 5 |
| Yield, vol. % of feed | | | | | |
| Gasoline | 45.0 | 51.0 | 56.0 | 61.0 | 64.0 |
| Diesel oil | 35.0 | 29.0 | 24.0 | 20.0 | 16.0 |
| Tar acids | 2.0 | 1.0 | -- | - | - |
| Tar bases | 1.0 | 0.5 | -- | - | - |
| Residue | 12.0 | 12.0 | 13.0 | 11.5 | 12.0 |
| Gas (including losses) | 4.5 | 6.5 | 7.0 | 7.5 | 8.0 |
| Sulfur, wt. % of feed | 0.0489 | 0.0210 | 0.014 | 0.0135 | 0.0136 |
| Nitrogen, wt. % of feed | 0.0924 | 0.0442 | 0.0321 | 0.0201 | 0.0163 |
| Composition of gasoline, vol. % | | | | | |
| Aromatics | 33.5 | 35.0 | 34.0 | 32.0 | 33.0 |
| Naphthenes | 10.0 | 9.0 | 10.5 | 10.0 | 10.0 |
| Olefins | 2.0 | 3.0 | 2.0 | 2.0 | 4.0 |
| Isoparaffins | 25.5 | 26.0 | 26.0 | 27.0 | 25.0 |
| N-paraffins | 29.0 | 27.0 | 27.5 | 29.0 | 28.0 |
| Diesel index of diesel oil | 40.0 | 37.5 | 34.0 | 31.0 | 28.0 |
| Isobutane / N-butane | 1.0 | 1.25 | 1.45 | 1.51 | 1.75 |

Table III. Influence of Pressure on Yield and Composition of Gasoline

| Yield and Hydrocarbon Types, Vol. % | Temperature, °C. | Pressure, psi. 1000 | 1250 | 1500 | 1750 | 2000 | 2250 | 2500 | 2750 | 3000 |
|---|---|---|---|---|---|---|---|---|---|---|
| Yield | 400 | 15.0 | 36.0 | 45.0 | 48.0 | 50.0 | 54.0 | 58.0 | 63.0 | 68.0 |
| Aromatics | 400 | 33.5 | 36.0 | 33.5 | 46.0 | 50.0 | 46.5 | 40.0 | 33.5 | 28.0 |
| Naphthenes | 400 | 10.0 | 9.5 | 10.0 | 10.5 | 10.0 | 18.5 | 24.0 | 28.5 | 31.0 |
| Olefins | 400 | 5.5 | 3.0 | 2.0 | 1.5 | 2.0 | 3.5 | 2.5 | 4.0 | 3.5 |
| Isoparaffins | 400 | 24.0 | 24.0 | 25.5 | 19.0 | 20.0 | 18.5 | 19.0 | 20.5 | 25.5 |
| N-paraffins | 400 | 27.0 | 27.5 | 29.0 | 23.0 | 18.0 | 13.0 | 14.5 | 13.5 | 12.0 |
| Yield | 450 | 36.0 | 49.0 | 56.0 | 58.0 | 60.0 | 62.0 | 66.0 | 69.0 | 73.0 |
| Aromatics | 450 | 36.0 | 32.5 | 34.0 | 44.0 | 60.0 | 56.0 | 47.0 | 39.0 | 33.0 |
| Naphthenes | 450 | 11.0 | 10.0 | 10.5 | 12.0 | 12.5 | 15.0 | 23.0 | 29.0 | 35.0 |
| Olefins | 450 | 3.0 | 3.5 | 2.0 | 1.0 | 1.0 | 1.0 | 1.0 | 1.0 | 1.0 |
| Isoparaffins | 450 | 23.5 | 26.5 | 26.0 | 21.0 | 13.0 | 14.0 | 15.5 | 19.0 | 22.0 |
| N-paraffins | 450 | 26.5 | 27.5 | 27.5 | 22.0 | 14.0 | 14.0 | 13.5 | 12.0 | 9.0 |
| Yield | 500 | 44.0 | 54.0 | 64.0 | 66.0 | 68.0 | 69.0 | 71.0 | 74.0 | 77.0 |
| Aromatics | 500 | 36.5 | 33.0 | 33.0 | 44.0 | 50.0 | 49.0 | 41.0 | 32.5 | 26.0 |
| Naphthenes | 500 | 11.5 | 10.0 | 10.0 | 11.0 | 12.5 | 13.0 | 19.0 | 25.5 | 34.0 |
| Olefins | 500 | 4.0 | 5.0 | 4.0 | 4.5 | 3.0 | 4.5 | 2.0 | 3.0 | 2.0 |
| Isoparaffins | 500 | 23.0 | 25.0 | 25.0 | 19.5 | 17.5 | 17.0 | 21.0 | 23.5 | 26.0 |
| N-paraffins | 500 | 25.0 | 27.0 | 28.0 | 21.0 | 17.0 | 16.5 | 17.0 | 15.5 | 12.0 |

Table IV. Comparison of Yield and Composition of Gasolines (Gasoline 1 at 450°C, 2000 psi, 10 hours and Gasoline 2 at 500°C, 3000 psi, and 5 hours, both from Tar)

| | Gasoline 1 | Gasoline 2 | Regular grade gasoline from petroleum | Premium grade gasoline from petroleum |
|---|---|---|---|---|
| Yield, vol. % of feed | 60.0 | 77.0 | - | - |
| Hydrocarbon composition, vol. % | | | | |
| Aromatics | 60.0 | 26.0 | 33.0 | 34.0 |
| Naphthenes | 12.5 | 34.0 | 18.0 | 12.0 |
| Olefins | 1.0 | 2.0 | 11.0 | 14.0 |
| Isoparaffins | 13.0 | 26.0 | 22.0 | 28.0 |
| N-paraffins | 14.0 | 12.0 | 16.0 | 12.0 |

Literature Cited

1. Gordon, K., J. Inst. Fuel 9, 69 (1935); 20, 42 (1946); 21, 53 (1947).

2. Pier, M., Z. ElectroChem. 53, No. 5, 291 (1949).

3. Weisz, P. B., Prater, C. D., Advan. Catalysis 9, 575 (1957).

4. Keulemans, A. I. M., Voge, H. H., J. Phys. Chem. 63, 476 (1959).

5. Flinn, R. A., Larson, O. A., Beuther, H., Ind. Eng. Chem. 52, 152 (1960).

6. Archibald, R. C., Greensfelder, B. S., Holzman, G., Rowf, D. H., Ibid., 52, 745 (1960).

7. Carpenter, H. C., Cottingham, P. L., Frost, C. M., Fowkes, W. W., Bureau of Mines Report of Investigation No. 6237 (1963).

8. Alpert, S. P., Johanson, E. S., Schuman, S. C., Chem. Eng. Progress 60, No. 6, 35 (1964).

9. Rutkowski, M., Zesz. Nauk. Politech. Wrol. Chem. 12, 3 (1965).

10. Katsobashvili, Ya. R., Elbert, E. I., Coke and Chemistry, U.S.S.R. 1, 41 (1966).

11. Zielke, C. W., Struck, R. T., Evans, J. M., Costanza, C. P., Gorin, E., Ind. Eng. Chem. 5, 151 and 158 (1966).

1 CERAMIC FURNACE
2 LIQUID SAMPLING TUBE
3 GAS SAMPLING TUBE
4 THERMOWELL
5 COOLING COIL
6 COOLING JACKET
7 MAGNETIC DRIVE ASSEMBLY
8 SHAFT
9 IMPELLER

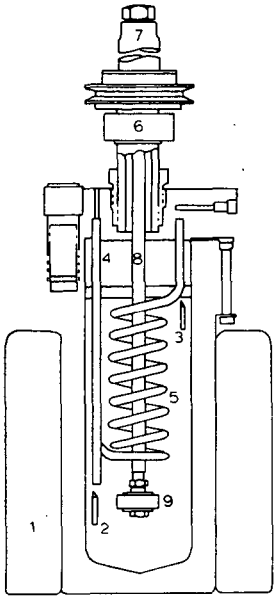


**Figure 1. Assembly of equipment**

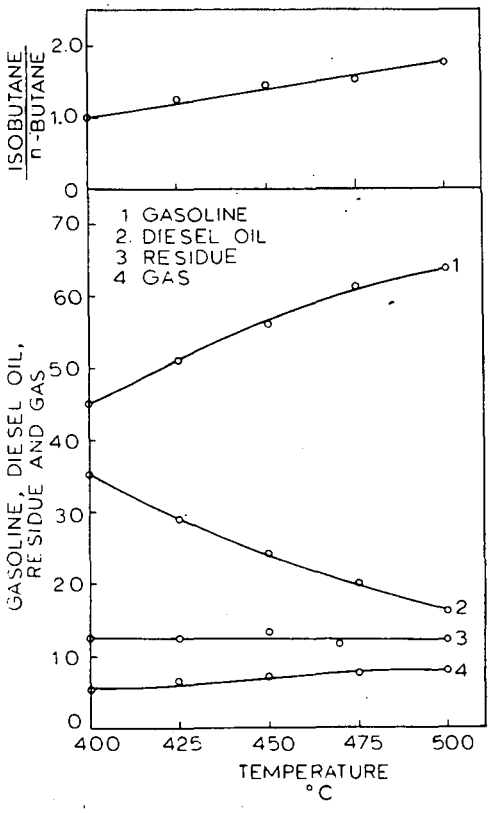


Figure 2. Effect of temperature on product distribution
Pressure, 1500 psi.
Reaction time, 13 hrs. at 400°C., 12 hrs. at 425°C.,
10 hrs. at 450°C., 8 hrs. at 475°C.,
5 hrs. at 500°C.

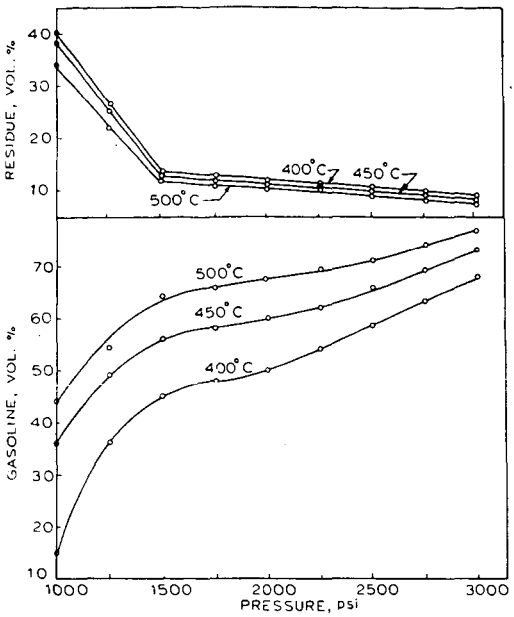


Figure 3. Effect of pressure on product distribution
Reaction time, 13 hrs. at 400°C.
10 hrs. at 450°C.
5 hrs. at 500°C.

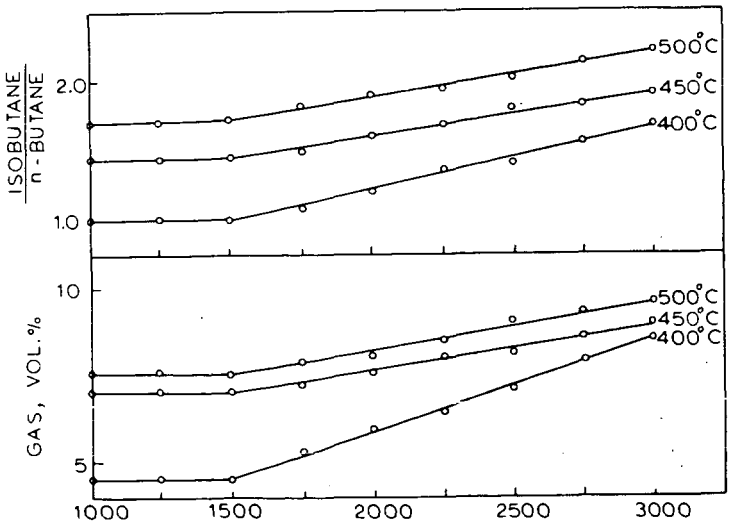


**Figure 4. Effect of pressure on product distribution**

**Reaction time, 13 hrs. at 400 C**
**10 hrs. at 450 C**
**5 hrs. at 500 C**

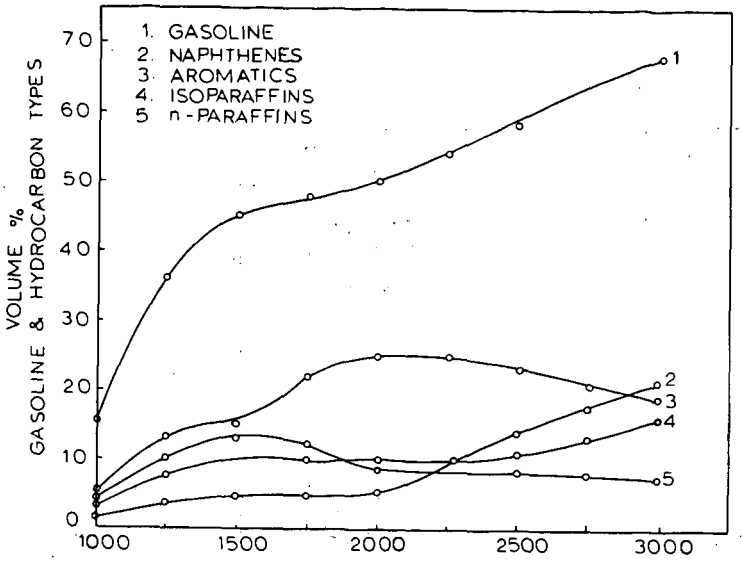


Figure 5. Effect of pressure on the yield of gasoline and hydrocarbon types - Temperature, 400 C

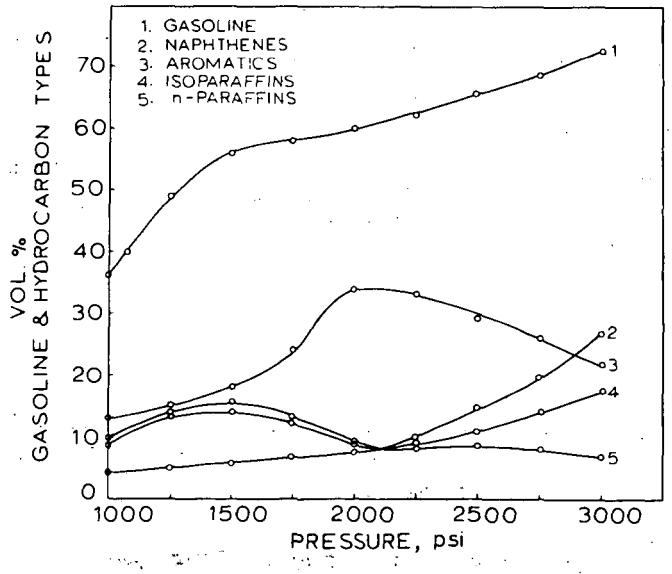


Figure 6. Effect of pressure on the yield of gasoline and hydrocarbon types - Temperature, 450 C

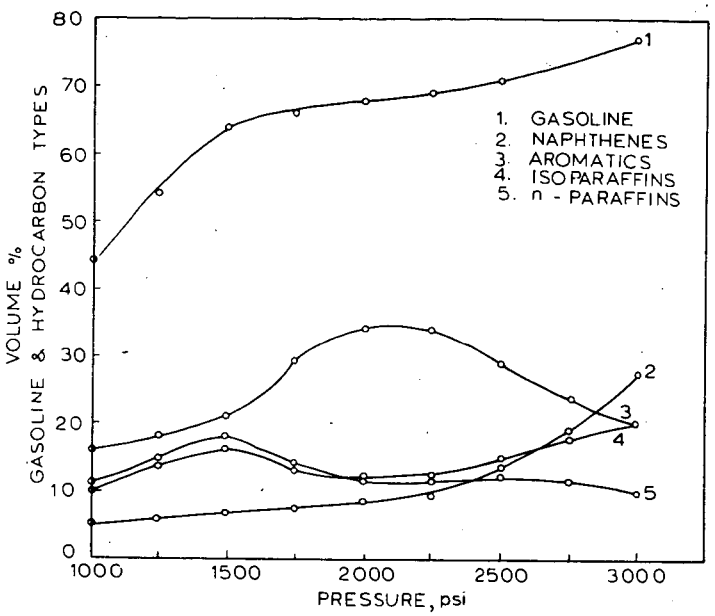


Figure 7. Effect of pressure on the yield of gasoline and hydrocarbon types - Temperature, 500 C

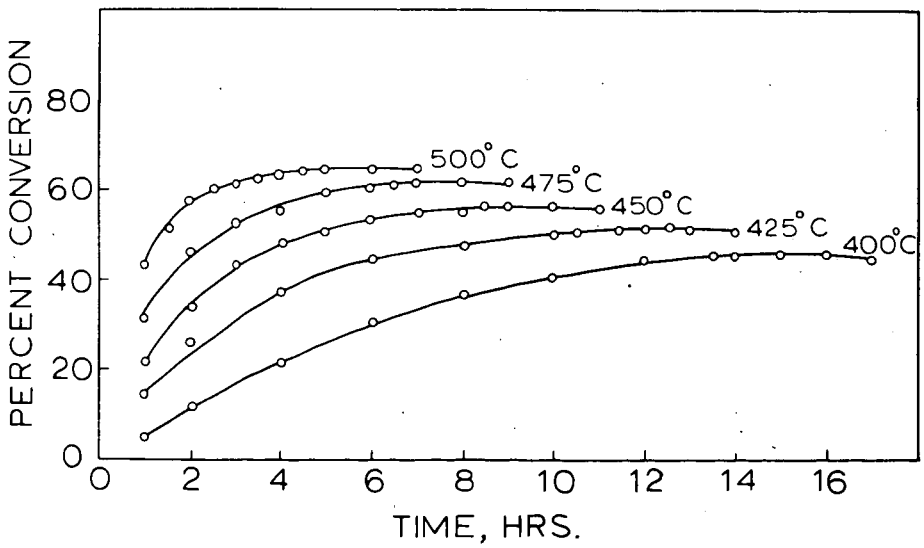


Figure 8. Effect of reaction time on gasoline formation Pressure, 1500 psi

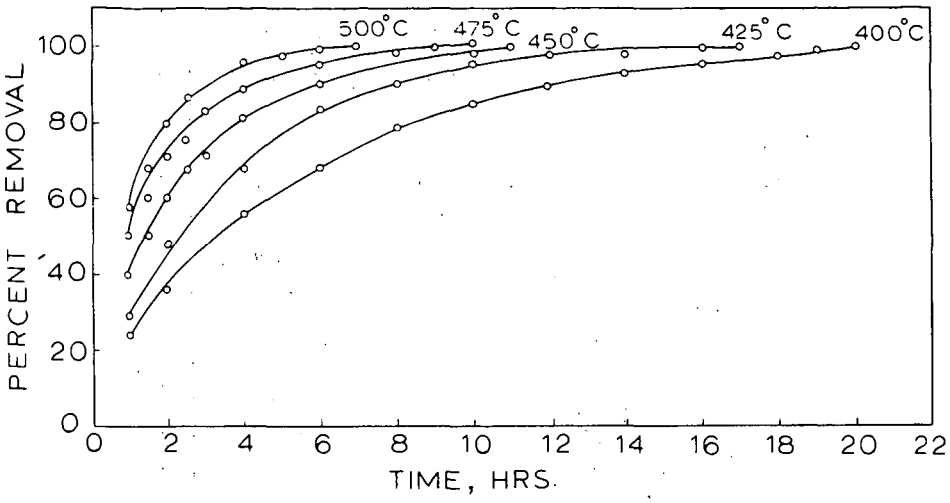


Figure 9. Effect of reaction time on desulphurization
Pressure, 1500 psi.

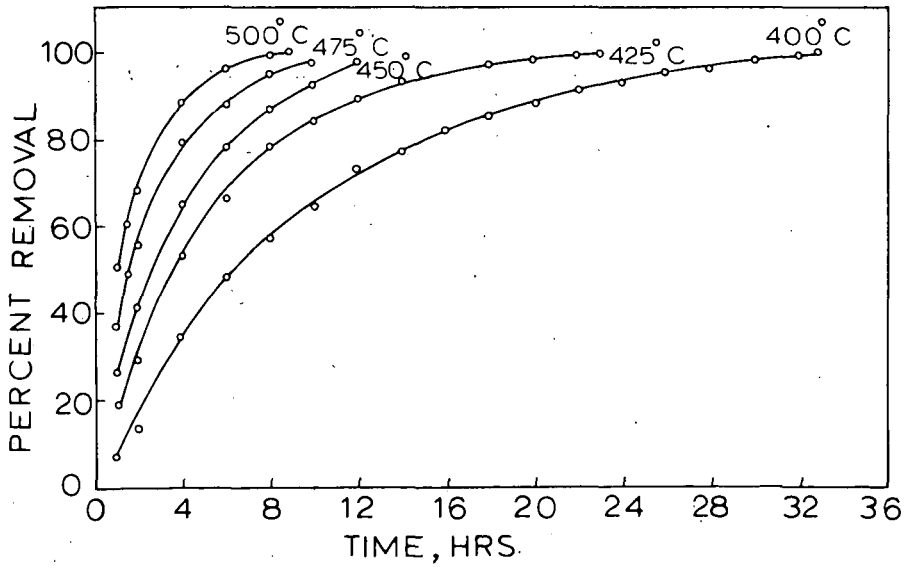


**Figure 10. Effect of reaction time on denitrogenation**
**Pressure, 1500 psi**

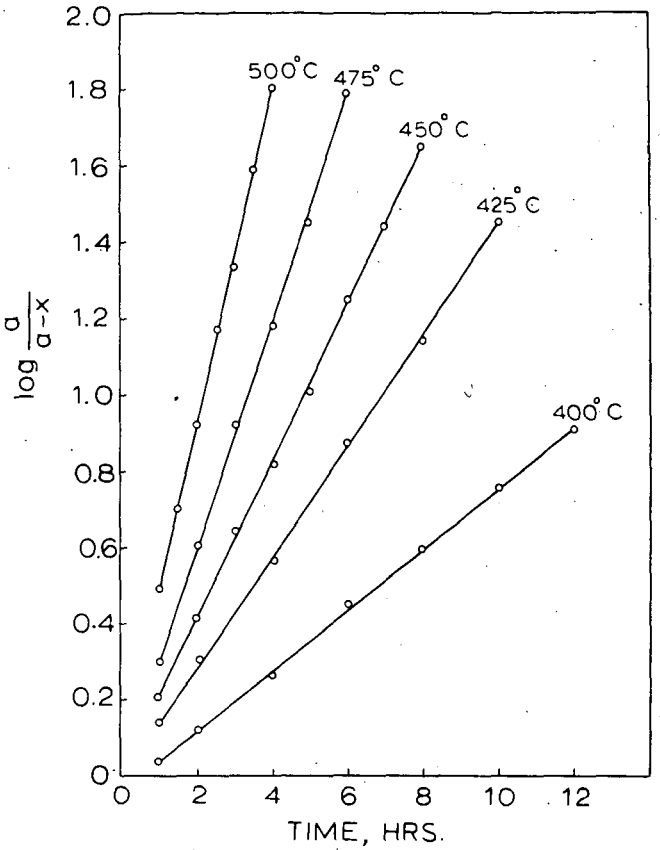


Figure 11. Plot of first-order equation for gasoline formation

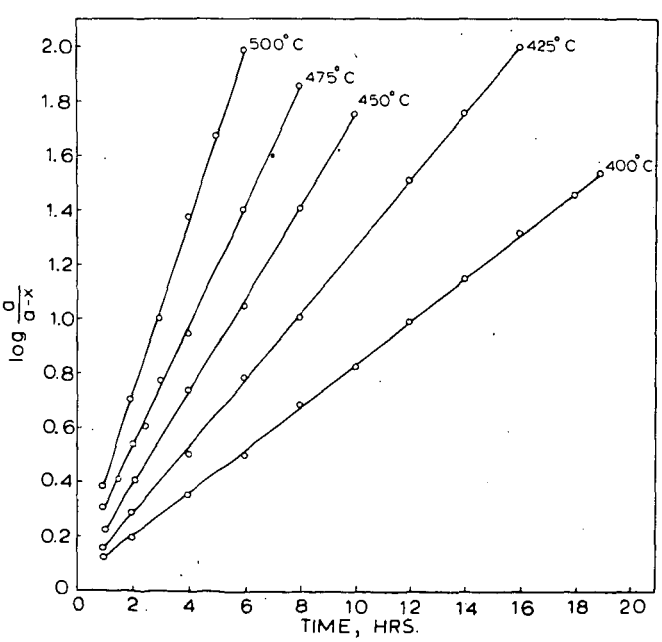


Figure 12. Plot of first-order equation for desulphurization.

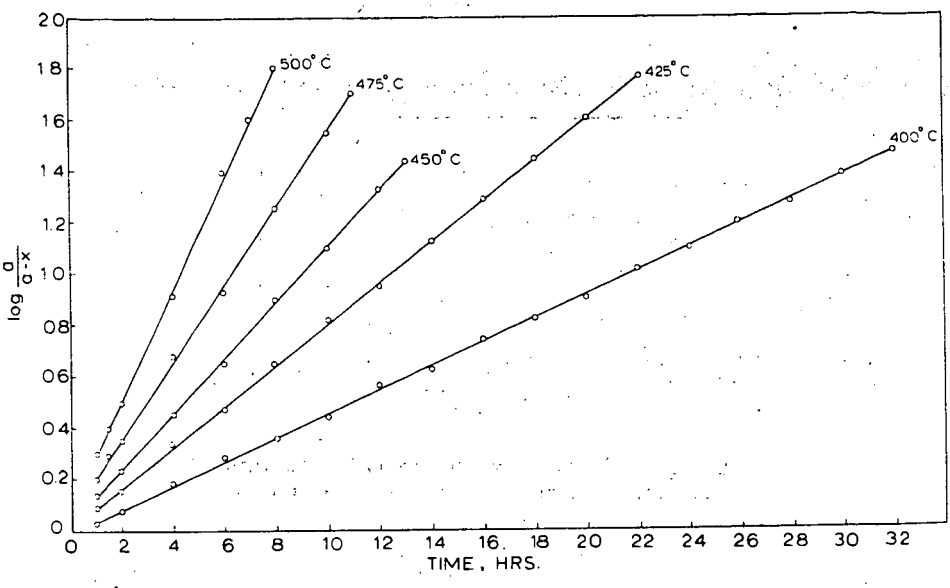


Figure 13. Plot of first-order equation for denitrogenation

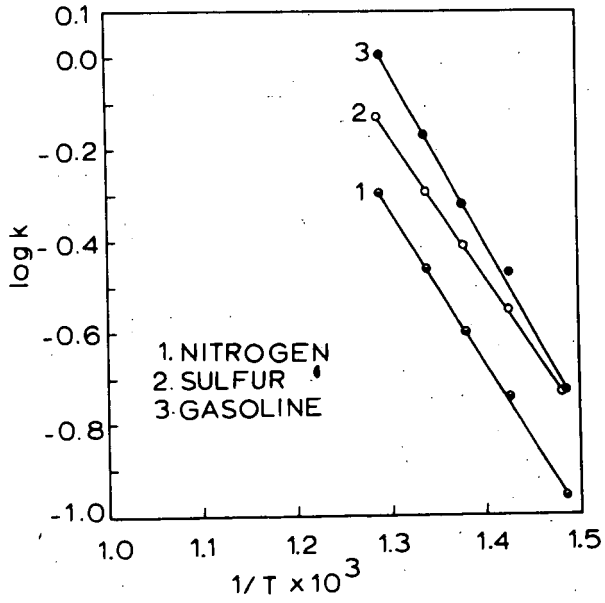


**Figure 14. Arrhenius plot for gasoline formation, desulphurization and denitrogenation**

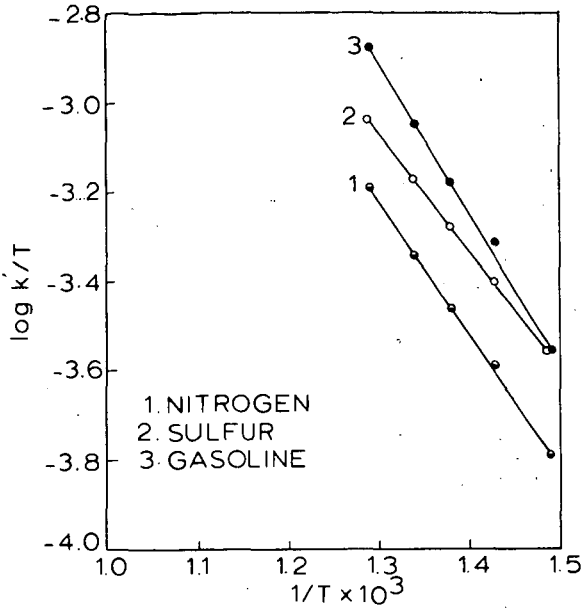


**Figure 15. Eyring plot for gasoline formation, desulphurization and denitrogenation.**

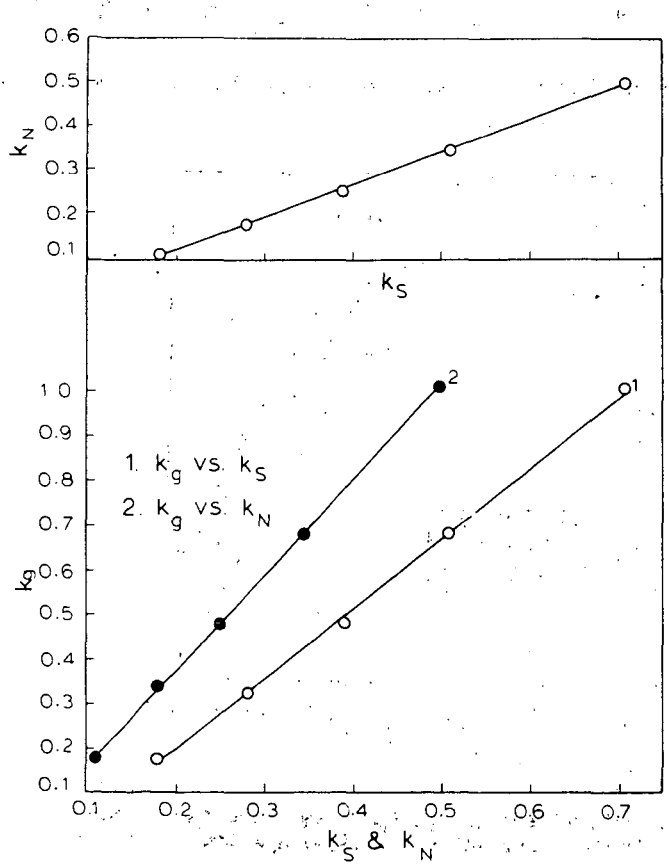


Figure 16. Relationship between rate constants
Pressure, 1500 psi.
Temperature, 400°, 425°, 450°, 475° and 500°C.

# DELAYED COKING OF LOW-TEMPERATURE LIGNITE PITCH

John S. Berber, Richard L. Rice, and Robert L. Lynch

U. S. Department of the Interior, Bureau of Mines,
Morgantown Coal Research Center, Morgantown, West Virginia

This paper is one of a series on the upgrading and utilization of various low-temperature tar fractions. Previous publications gave details on the preparation of biodegradable detergents from the olefin fraction (1), phthalic and maleic anhydrides from the neutral oil (3), and carbon electrode binders from the thermal cracking of the pitch (2).

Processing of petroleum residuals by delayed coking has been practiced commercially for a number of years (6). Pilot-plant studies have also been carried out on coke oven pitch (7) and a low-temperature tar topped to a temperature of 425° F (4). We believe this is the first effort to extend delayed coking to a low-temperature tar pitch.

## MATERIAL, EQUIPMENT, AND PROCESS DESCRIPTION

The tar was produced by the Texas Power & Light Company from a Texas lignite carbonized at 950° F in a fluidized bed. The pitch used in this study was obtained by distilling the crude tar under vacuum to an atmospheric boiling point of 630° F and amounted to 45 percent of the tar. Chemical and physical properties of the pitch are given in Table 1.

The delayed coking apparatus consists of a steel drum (C, see Figure 1) fabricated from a 5-foot length of 8-inch carbon steel pipe. The drum is flanged at the top and bottom ends to make the removal of the coke and cleaning easy. Coke removal is facilitated by use of a tilting drum. The coking drum is heated electrically (15.6 KW max). The pitch feed tank (A) was made from a 15-inch length of 8-inch carbon steel pipe and a cone, with a 1/2-inch coupling at the apex, is welded to the bottom of the 8-inch pipe and the top is open. The pitch tank is electrically heated by a 1.8 KW heater.

The pitch to be coked is ground and liquified in the pitch feed tank by heating to 400° F. The liquid pitch flows to the pitch feed pump (B), a small gear pump driven by an electric motor and hydraulic speed control (J), and is pumped through the pitch line preheater (F) which raises the temperature to about 485° F. The pitch is then fed to the delayed coking drum (C) which is maintained at the desired coking temperature. The pitch remains in the coking drum for several hours while the volatile matters are driven off. The volatiles are fed to an oil and gas condenser (D) and oil is collected in the bottom of the separator (E), and the gas is water scrubbed (H). The gas is then metered (G) and vented. A small tank (K) is tied into the pitch system in such a way that the pitch can be flushed out of the pump with a crude tar distillate fraction. Flushing the pump with crude tar before cooling prevents pitch solidification and simplifies restart.

A photograph of the apparatus is given in Figure 2.

The oil from the separator is vacuum distilled to about 750° F which yields an aromatic-rich distillate and a residue. The distillate can be catalytically oxidized to phthalic and maleic anhydrides while the residue, pitch, can be used as a binder for carbon electrodes, road paving, roofing, or piping material, depending on its specifications, such as softening point, carbon-hydrogen ratio, hydrogen content, and coking value.

## RESULTS AND DISCUSSION

This investigation was conducted at temperatures from 800° to 1,200° F and at atmospheric pressure. The coke yield ranged from 25 percent at 800° F to 45 percent at 1,200° F (Figure 3). This increase in yield is due to the higher degradation of the feed pitch at elevated temperatures. The product appeared darker, smoother, and char-like at 800° F, while at 1,200° F the coke had the silver-grey color typical of coke (Figures 4 and 5).

The ash content of the coke, as shown in Figure 6, was the same over the entire range of coking temperatures. The iron content of the coke (Figure 7) also was constant at all temperatures.

The sulfur content of the coke decreased slightly with the increasing temperature, Figure 8, indicating that, at higher temperatures, more of the sulfur was being converted to gas. It has been reported that delayed coke can be used as fuel for generating electric power (5). The relatively low sulfur content of this coke, 0.80 percent, should make it especially attractive as a fuel in view of present air pollution standards.

The coke obtained from this process can also be calcined and used as aggregate in the production of metallurgical electrodes, although the ash is slightly higher than the ash of petroleum coke which is currently used. It is desirable to have an ash content below 0.5 percent in the coke. The coke loses 15 percent by weight when calcined to 2,000° F.

The oil yield is a function of coking temperature and varied from 43 percent of the feed pitch at 800° F to 17 percent at 1,200° F (Figure 3). The specific gravity of the oil was about 0.95 at 800° F and 1.18 at 1,200° F (Figure 9). This oil, when distilled to 720° F, gave a distillate containing from 15 to 25 percent combined acids and bases with the remainder consisting of a neutral oil. The F.I.A. analysis of a typical neutral oil showed 89.2 percent aromatics, 6.9 percent olefins, and 3.9 percent paraffins. The vapor-phase catalytic oxidation of the neutral oil yielded better than 30 percent phthalic and maleic anhydrides. The distillation residue from the oil proved to be a suitable binder for metallurgical electrodes. A detailed evaluation of its use as a binder, as well as the coke as an aggregate, is in progress and will be reported in a future publication.

The gas yield was 17 percent at 800° F and increased to 39 percent at 1,200° F (Figure 3). The effect of coking temperature on the ethylene-to-ethane ratio is shown in Figure 10. This is probably due to dehydrogenation and thermal cracking. In addition, an increase in coking temperature is accompanied by a decrease in the methane-to-hydrogen ratio (shown in Figure 11). This ratio drops from 8:1 at 800° F to about 2:1 at 1,150° F. A typical analysis of gas obtained at 950° F is given in Table II.

## CONCLUSIONS

This work has shown that the commercial value of lignite pitch is increased by coking. The coking operation yields three products: oil, gas, and coke. The oil upon distillation is a valuable chemical intermediate. The coke could be used as an aggregate for metallurgical electrodes, other graphite products, and as a low-sulfur fuel. The gas is a possible substitute for natural gas or a source of hydrogen if subjected to a steam reforming process. Ethylene could also be recovered from the gas stream and used as a raw material.

## LITERATURE CITED

1. Berber, J. S., Rahfuse, R. V., Wainwright, H. W., Ind. Eng. Chem., Prod. Res. Develop. 4, 242 (1965).

2. Berber, J. S., Rice, R. L., Fortney, D. R., Ind. Eng. Chem., Prod. Res. Develop. 6, 197 (1967).

3. Berber, J. S., Rice, R. L., Hiser, A. L., Wainwright, H. W., Bur. Mines Rept. Invest. 6916, 1967, 17 pp.

4. Dell, M. B., Ind. Eng. Chem. 51, 1297 (1959).

5. Donnelly, F. J., Barbour, L. T., Hydrocarbon Process. 45, 221 (1966).

6. Martin, S. W., Wills, L. E., Ch. in "Advances in Petroleum Chemistry and Refining," v. II, ed. by J. J. McKetta, Jr., and K. A. Kobe, pp. 367-387, Interscience Publications, Inc., New York, 1959.

7. Ibid., pp. 379-380.

Table I. Properties of Pitch Feed

| | |
|---|---|
| Ultimate analysis: | As received |
| Carbon, % | 84.72 |
| Hydrogen, % | 8.53 |
| Nitrogen, % | 0.87 |
| Oxygen, % | 4.62 |
| Sulfur, % | 0.90 |
| Chlorine, % | 0.01 |
| Moisture, % | 0.00 |
| Flash point, ° F | 510 |
| Softening point (R & B) glycerin, ° C | 90 |
| Softening point (cube in glycerin), ° C | 105 |
| Penetration at 77 ° F, 100 grams, 5 seconds | 0 |
| Specific gravity, 25 ° C/25 ° C | 1.128 |
| Ash, % | 0.35 |
| Water, % | 0.00 |
| Ductility, cm at 77 ° F | 0 |
| Bitumen, soluble in $CS_2$ | 78.80 |
| Free carbon | 20.85 |
| Distillation: | |
| To 300 ° C, % | 6.40 |
| Softening point of residue (R & B), ° C | 90 |
| Sulfonation index of distillate to 300 ° C | 0 |
| Conradson carbon, % | 20.81 |

Table II. Composition of Gas at a Coking Temperature of 950° F

| Component | Volume-percent |
|---|---|
| $CO_2$ | 0.74 |
| CO | 4.91 |
| $H_2$ | 7.67 |
| $CH_4$ | 43.83 |
| $C_2H_6$ | 13.97 |
| $C_2H_4$ | 9.94 |
| $C_3H_8$ | 13.54 |
| $C_4^+$ | 5.40 |

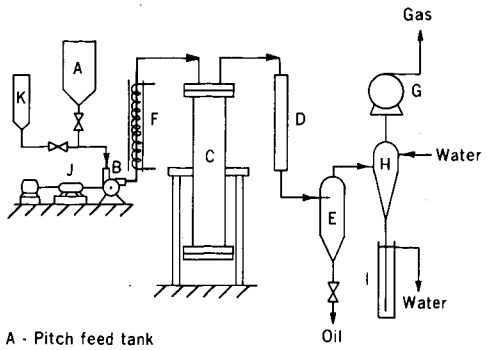


A - Pitch feed tank
B - Pitch feed pump
C - Delayed coking drum
D - Gas and oil cooler
E - Oil separator
F - Pitch line preheater
G - Wet test meter
H - Gas water scrubber
I - Scrubber seal pot
J - Hydraulic speed control
K - Pump flushing oil tank

FIGURE 1. - Flowsheet of Delayed Coking Process.

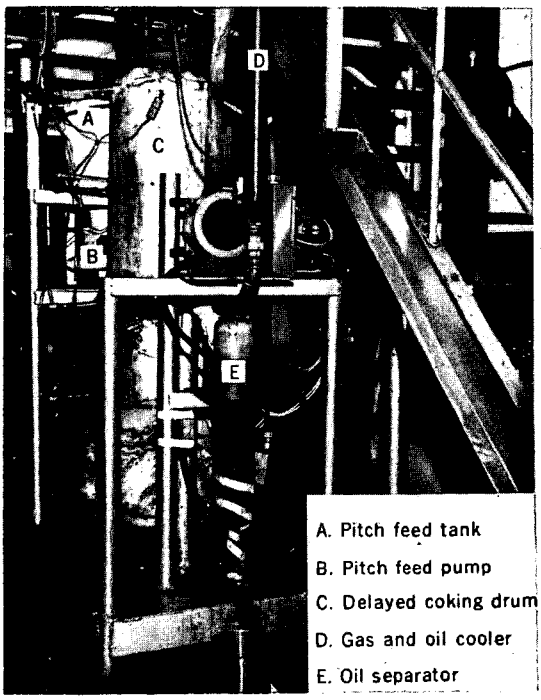


FIGURE 2. - The Delayed Coking Apparatus.

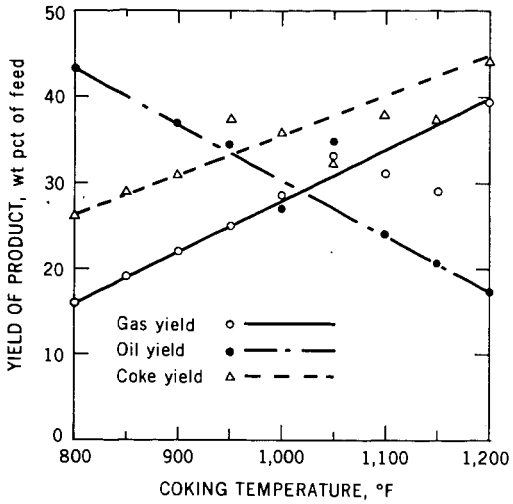


FIGURE 3. - Effect of Temperature on Product Distribution.

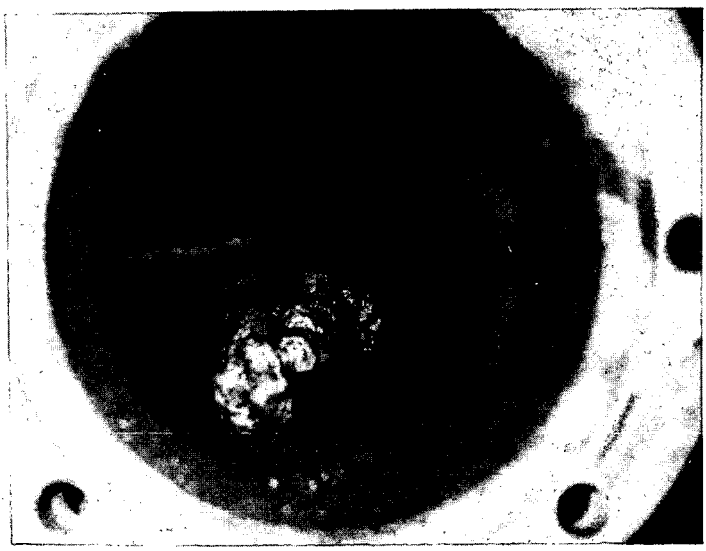

FIGURE 4. - Coke at the Top End of the Drum.

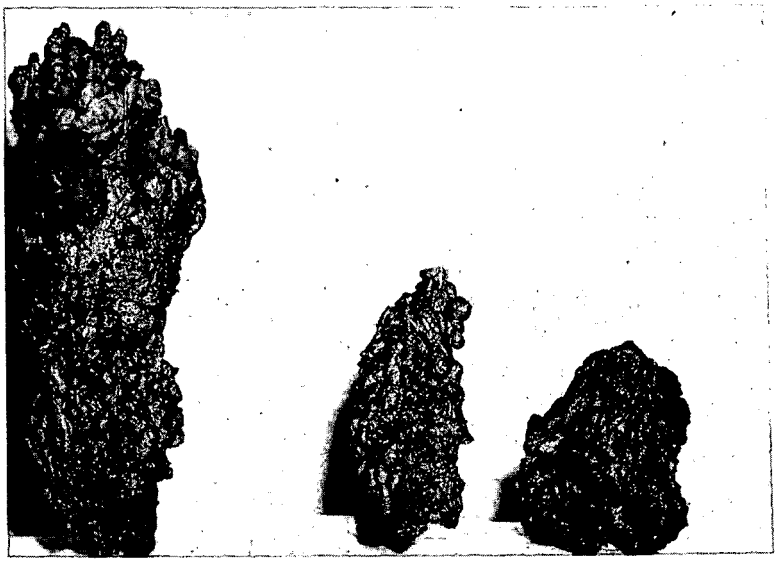

FIGURE 5. - Coke as Taken From Drum.

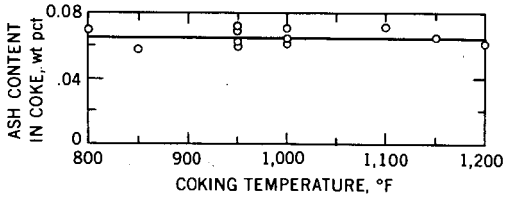


FIGURE 6. - Coking Temperature vs. Ash Content of Coke.

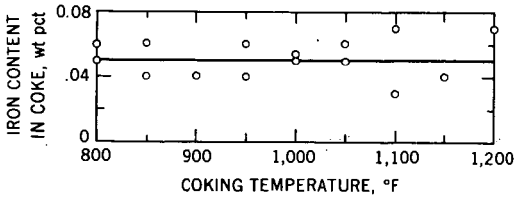


FIGURE 7. - Coking Temperature vs. Iron Content of Coke.

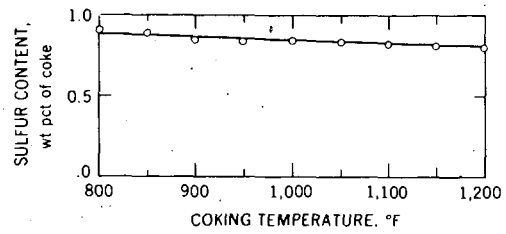


FIGURE 8. - Coking Temperature vs. Sulfur Content of Coke.

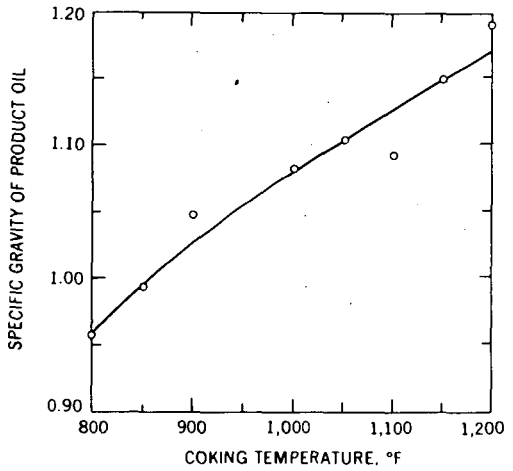


FIGURE 9. - Effect of Temperature on Specific Gravity of Product Oil.

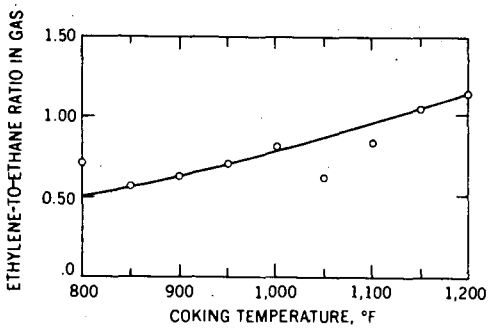


FIGURE 10. - Effect of Temperature on Ethylene-to-Ethane Ratio.

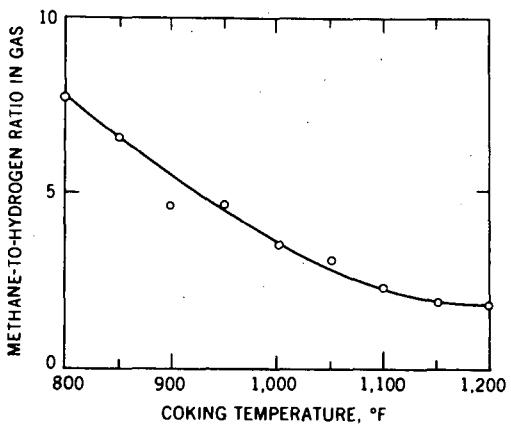


FIGURE 11. - Effect of Temperature on Methane-to-Hydrogen Ratio.